Ab initio and Direct Quasiclassical Trajectory Study of the $F + CH_4 \rightarrow HF + CH_3$ and $F + C_2H_6 \rightarrow HF + C_2H_5$ Reactions

Paula J. E. Weiss

Thesis submitted to the faculty of the Virginia Polytechnic Institute and State University
in partial fulfillment of the requirements for the degree of

Master of Science
In
Chemistry

Dr. Diego Troya, Chair
Dr. T. Daniel Crawford
Dr. Richard Gandour
Dr. John Morris
Dr. Edward Valeev

September 25, 2007
Blacksburg, Virginia

Keywords: specific reaction parameter semiempirical Hamiltonian, quasiclassical trajectory study, direct dynamics, potential energy surface

Ab initio and Direct Quasiclassical Trajectory Study of the $F + CH_4 \rightarrow HF + CH_3$ and $F + C_2H_6 \rightarrow HF + C_2H_5$ Reactions

Paula J. E. Weiss

ABSTRACT

The reparametization of semiempirical Hamiltonians is an emerging method used in direct dynamics studies. The use of semiempirical Hamiltonians in direct dynamics studies diminishes the computational cost of trajectory calculations and negates the need for an analytical potential energy surface when performing reaction dynamics studies. The reparametization of semiempirical Hamiltonians increases the agreement with experiment and high level *ab initio* theory. We have chosen to create one set of new parameters that apply to two related reactions, $F + CH_4 \rightarrow HF + CH_3$ and $F + C_2H_6 \rightarrow HF + C_2H_5$. We have performed an electronic structure study for these reactions. The *ab initio* data obtained from the electronic structure study is then used as the reference for a reparametization of the PM3 Hamiltonian. The reparametization has improved the *ab initio* and PM3 reaction energy and potential energy surface scan agreement. This new set of parameters for PM3 (SRP-PM3) is used to perform a direct quasiclassical trajectory study of the reactions. The vibrational and rotational HF distributions calculated using SRP-PM3 are compared with experiments. We have observed an improvement in the agreement with experimental vibrational distributions but have seen no change in the rotational distributions.

Acknowledgments

There are multiple people that I would to thank for helping complete this work:

- My advisor, Dr. Diego Troya, for teaching me everything that I know about computational chemistry.
- My group members: Will Alexander, Josh Layfield and Uros Tasic for the advice that they have given me.
- All of the members of my committee.
- The very special friends that I have made these past two years: Jessica Lu, Joan Zapiter, Avi Jain, and Hiro Motegi who have always been there for me.
- My parents for always giving me their support.
- Most importantly I would like thank my husband, who I don't think that I would have survived without.

Table of Contents

List of Figures

List of Tables

Chapter 1 Introduction

One of the main goals of chemistry is to understand what occurs at the molecular level when chemical and/or physical changes occur. In reaction dynamics studies, we examine the changes that occur at the atomic level as a reaction proceeds from reactants to products. Experiments can generate a wealth of information about the dynamics of reactions, but a complete understanding of a reaction might be difficult due to limitations in experimental technology. By using theory, we can probe aspects of reactions not available for study by experimentalists. Reaction dynamics can be studied in the gas phase, in solution, and on surfaces. This work will deal with reactions in the gas phase. We note that gas phase studies are in principle less complicated than when condensed phases are involved because interactions with the environment are minimized.

This work describes our efforts to describe the dynamics of the $F + CH_4 \rightarrow HF + CH_3$ and $F + C_2H_6 \rightarrow HF + C_2H_5$ reactions. In this chapter, we first review the available information about these reactions. We then describe some of the theoretical aspects of our approach to investigate reaction dynamics, including the concept of a potential energy surface, and the classical trajectory method. In Chapter 2, we describe electronic structure calculations of the potential energy surfaces of these reactions. In Chapter 3, we show a modification of a semiempirical Hamiltonian to make it more accurate for the $F + CH_4 \rightarrow HF + CH_3$ and $F + C_2H_6 \rightarrow HF + C_2H_5$ reactions. Chapter 4 presents the results of trajectory calculations of the reactions' dynamics using the semiempirical Hamiltonian derived in this work. Finally, Chapter 5 gathers our main conclusions.

1.1 Literature Review of the $F+CH_4$ and $F+C_2H_6$ Reactions

The $F + CH_4 \rightarrow HF + CH_3$ reaction has been well explored experimentally. This system is of interest for multiple reasons. The HF product shows an inversion of the vibrational population, which peaks at v=2, making the reaction interesting in the field of chemical lasers.[1] This inversion in population is in part due to the exothermicity of the reaction ($\Delta_r H^{0K} = -32.1$ kcal/mol)[2], which is channeled mostly into product vibration.

Some of the first experimental studies were performed by Nazar and Polanyi.[3] They used infrared (IR) chemiluminescence to probe the HF product. They identified this reaction as a heavy-light-heavy (H+LH) system. They note there is a tendency in H + LH reactions for the L to bounce back to the departing H after its encounter with the attacking H before forming the new HL product. Wickrammaaratchi *et al*.[4] used IR chemiluminescence to detect HF products. They determined that direct hydrogen abstraction occurs and that secondary processes are unimportant. Sugawara *et al*.[5] observed the CH_3 product in a bulk experiment using spectroscopic detection. They observed vibrational and rotational distributions for CH_3. They concluded that the CH_3 product was rotationally cold. Maneshkarimi *et al*.[6] used IR chemiluminescence to study the effect of the secondary reaction, $F + CH_3 \rightarrow HF + CH_2$. When there was an excess of fluorine atoms in the system, the authors noted a change in the vibrational distribution of HF which was attributed to the secondary reaction.

Harper *et al*.[7] used high-resolution IR laser dopplerimetry to study the angular distribution of the reaction. They found that forward/backward scattering of the HF product is more likely to occur than side scattering. They have also used high-resolution IR laser absorption to study the state-to-state reactive scattering of the reaction.[8] They investigated the quantum resolved dynamics under crossed supersonic jet conditions, which eliminates contributions from collisional relaxation effects and secondary reactions. They were able to measure nascent rovibrational HF product state distributions, including v=0. From that information, they inferred that the transition state has a bent geometry, and that the reaction has an early reaction barrier.

Shui *et al*.[9] used velocity map ion imaging to measure the reaction excitation function. They found that the excitation function has a fast rise to its maximum around 1.3 kcal/mol, and then a slightly slower decline as the collision energy continues to increase up to 7.3 kcal/mol. Also Shiu *et al*.[10] discovered reactive resonance in the reaction. Merritt *et al*.[11] used high-resolution IR laser spectroscopy to study the exit-channel complex of the reaction. They found the exit channel complex, $CH_3 \cdots HF$, to have a C_{3v} structure. This complex is associated with a shallow well in the potential energy surface due to the stabilizing interactions of the dipole moment of the HF moiety with the CH_3 radical.

Over the years, several groups have determined thermal rate constants for the F + $CH_4 \rightarrow HF + CH_3$ reaction. Fettis *et al.*[12] and Foon and Reid[13] determined the activation energy using a competitive technique and gas chromatography. Williams and Rowland[14] obtained rate constants using a relative rate technique and gas chromatography. Setser *et al.*[15-17] performed several experiments using IR chemiluminescence to determine relative rate constants and vibrational distributions. Moore and Smith[18] measured rate constants at room temperature using Fourier transform infrared (FTIR) spectroscopy and a relative rate technique. Persky[19] investigated the kinetics of the reaction in the temperature range 184-406 K. He used a competitive method to determine the temperature dependence of the rate constant. He found the Arrhenius plot (log(rate) vs 1/T) to be linear and determined the activation energy. Persky[20] has also studied the kinetic isotope effect of the reaction of fluorine atoms with CH_4 and CD_4 in the temperature range 183-298 K. He found that the ratio of the rate constant for the regular reaction vs. the reaction with the perdeuterated methane molecule to be $k_{F+CH4}/k_{F+CD4}=1.38\pm0.04$ at 298 K.

$F + CH_4 \rightarrow HF + CH_3$ is a prototypical reaction for the development of theoretical methods because there are relatively few electrons involved in the system, and there is a wealth of experimental information against which theory can be calibrated. Therefore, it is not surprising that several theoretical studies have been performed on the $F + CH_4 \rightarrow HF + CH_3$ reaction in recent years. Gauss[21] performed one of the first trajectory studies on the reaction. He used a three-parameter London-Eyring-Polanyi-Sato (LEPS) potential energy surface (PES) for the trajectory calculations. He examined the relationships between the reaction cross sections and collision energies, and found that the cross section increases with increasing collision energy. Davis *et al.*[22] performed a study of the reaction using *ab initio* and modified neglect of differential overlap (MNDO) methods. Geometries and frequencies were calculated with UMP2/6-311+G(2df,2dp) and single-point calculations were performed at the QCISD(T)/6-311++G(2df,2dp) level. Kornweitz *et al.*[23] performed a classical trajectory study on the reaction. They constructed a full-dimensional PES, which was a modification of an existing potential for the H + CH_4 reaction. The calculated vibrational distribution of the HF product was found to agree with experiments.

Corchado *et al*.[24, 25] performed *ab initio* reaction path and trajectory studies using two semiempirical surfaces. An *ab initio* study of the stationary points and reaction path of the PES was performed using MP2 and QCISD theory. Two potential energy surfaces were constructed. One surface was a specific reaction parameter (SRP) PM3, using reactant and product experimental properties as reference data. The other surface was a modification of the J1 surface[26] developed for the H + CH_4 reaction (MJ1) using *ab initio* saddle-point information (barrier height, geometry, and vibrational frequencies) as reference data. Both PESs exhibited an early linear transition state, and small reaction barriers. Rate constants were calculated for the temperature range 100-500 K.

Troya *et al*.[27] characterized the reaction dynamics and kinetics of F + CH_4 → HF + CH_3 using quasiclassical trajectories and transition state theory. They constructed an analytical reduced dimensionality PES treating the CH_3 group as a pseudoatom. The PES was constructed by fitting the *ab initio* points calculated at the PUMP4/6-311+G(2df,2pd) level to a triatomic analytical representation. They found that all reactive trajectories undergo a direct mechanism. They also found that the reaction has a linear saddle point and an early transition state and that the zero-point corrected barrier is negative due to the saddle point region in the PES being fairly flat. A quasiclassical trajectory study yielded HF vibrational and rotational distributions in good agreement with experiments. Several levels of transition state theory were used to calculate rate constants.

Roberto-Neto *et al*.[28] investigated the transition state structure, energetics, and rate constants of the reaction. BH&HLYP, MP2, and CCSD(T) theories, in combination with cc-pVXZ and aug-cc-pVXZ (where X=D,T,Q) basis sets were used for the study. The classical energy of reaction, enthalpy of reaction at 0 K, enthalpy of reaction at 298 K, classical barrier height, and vibrationally adiabatic ground state barrier height were calculated. The authors found the transition state to have a linear, quasi-linear, or bent structure depending on the method used. However the energy difference between the collinear and bent structures was very small.

Rangel *et al*.[29] constructed a potential energy surface and performed a kinetics and dynamics study for the reaction. The potential energy surface was constructed based on a previous surface[30], formulated in terms of stretching, valence bending, and out-of-

plane bending. Two surfaces were constructed to account for the two spin-orbit states of the fluorine atom. We note that the surface denoted PES-NOSO in that work will be used for comparison later in this work. Kinetic isotope effects, activation energy, and the reaction-path curvature were calculated. Thermal rate constants were calculated in the range 180-500 K.

Troya[31] performed an *ab initio* and direct quasiclassical trajectory study of the reaction using MP2, CCSD(T), and several semiempirical Hamiltonians. The parameters of the PM3 semiempirical Hamiltonian were optimized for the reaction. A direct quasiclassical trajectory study showed good agreement with experimental rovibrational distributions. A comparison with experimental excitation functions was made and good qualitative agreement was found.

Castillo *et al*.[32] performed an *ab initio* study with HF, MP2, QCISD, and QCISD(T) theory using different correlation consistent basis sets. The transition state geometry was found to be close to reactants. A PES was constructed using data calculated with MP2/aug-cc-pVDZ and MP2/SAC applying iterative and interpolation methods. This was a fully *ab initio* PES considering all degrees of freedom. A quasiclassical trajectory study was performed using this surface where predominately backward scattering was observed. The HF vibrational populations were found to depend upon the amount of vibrational energy disposed in the CH_3 coproduct.

Chu *et al*.[33] used first principles quantum dynamics to examine resonance in the reaction. They constructed two analytical potential energy surfaces with data calculated with QCISD/6-311++G(3df,2p) and QCISD(T)/6-311++G(3df,2p). They observed resonance at low collision energies with a lifetime of 26 fs. Wang *et al*.[34] examined the reactive resonance and formation mechanism of the reaction. An *ab initio* partial potential energy surface (PPES) was constructed using data from the minimum energy path (MEP) and vibrational levels along the whole reaction coordinate calculated with QCISD(T)/6-311++G(2df,2dp). It was observed that potential wells formed in the transition state region. They estimated the lifetime of the scattering resonance state, which was suggested by Liu, to be 0.07 ps.

Espinosa-Garcia *et al*.[1] created a PES that is a London-Eyring-Polanyi (LEP) type function to describe the stretching modes, augmented by the bending terms. This is a

recalibration of a previous surface by Rangel *et al*.[29] Calculated rate constants agree with experiments in the range 190-410 K. A quasiclassical trajectory study generated HF rovibrational distributions and state specific scattering distributions which agree with experiments.

In this work, in addition to revisiting the $F + CH_4 \rightarrow HF + CH_3$ reaction, we have simultaneously studied the homologue reaction $F + C_2H_6 \rightarrow HF + C_2H_5$. Fewer experimental or theoretical studies have been performed on this reaction in comparison with $F + CH_4$. Maricq *et al*.[35] used UV spectroscopy to determine the rate constant. Persky[36] examined the temperature dependence of the rate constant in the range 189-298 K. He used a competitive method with $F + CH_4$ as a reference reaction to determine an activation energy of 0.36 kcal/mol. Whitney *et al*.[37] investigated the state-to-state scattering dynamics using high-resolution IR laser absorption. Using a collision energy of 3.2 kcal/mol they were able to detect nascent rovibrationally resolved HF(v,J) product states. They concluded that the reaction has an early barrier. Several of the experimental studies mentioned earlier also studied the $F + C_2H_6 \rightarrow HF + C_2H_5$ reaction.[4, 12-18] Bottoni *et al*.[38] performed an *ab initio* study of the reaction. They used HF, MP2, MP4 theory, and 6-31G* and LANDL1DZ basis sets to calculate the reaction barrier. They observed the transition state having a bent geometry and being more reactant like.

1.2 Potential Energy Surfaces

The exact calculation of the dynamics of a chemical system requires solving the time-dependent Schrödinger equation for both nuclei and electrons. The motion of nuclei is much slower than that of electrons. Therefore, the motions of the nuclei and electrons can sometimes be separated. The mass of nuclei, being much heavier than that of electrons, causes this difference in the speed of motion. This separability of nuclear and electronic motion is referred to as the Born-Oppenheimer approximation.

1.2.1 Born-Oppenheimer Approximation

The Schrödinger equation[39], accounting for nuclei and electrons, can be written as

$$[H_{el} + T_n]\Psi(R,r) = E\Psi(R,r) \tag{1.1}$$

where H_{el} is the electronic Hamiltonian (which contains a term for nuclear repulsion), T_n is the kinetic energy operator for the nuclei, $\Psi(R,r)$ is the total wavefunction, R is the position of the nuclei relative to the center of mass of the molecule, r is the position of the electrons relative to the center of mass, and E is the energy.

The total molecular wavefunction[39] is a product of the electronic and nuclear terms

$$\Psi(R,r) = \Phi(R,r)\chi(R) \tag{1.2}$$

where $\Phi(R,r)$ is the electronic wavefunction and $\chi(R)$ is the nuclear wavefunction.

$\Phi(R,r)$ is the solution of the electronic Schrödinger equation[39]

$$H_{el}\Phi(R,r) = W(R)\Phi(R,r) \tag{1.3}$$

where $W(R)$ is the energy which is dependent on the nuclear coordinates R. This equation (Equation 1.3) is often referred to as the clamped nuclei approximation.

$\chi(R)$ is the solution of the nuclear Schrödinger equation[39]

$$[T_n + W(R)]\chi(R) = E\chi(R) \tag{1.4}$$

The potential energy felt by the nuclei can then be described as[39]

$$U(R) = W(R) \tag{1.5}$$

$U(R)$ is commonly referred to as the potential energy surface. Therefore, by solving the electronic Schrödinger equation for fixed nuclear positions, we have found the potential energy felt by the nuclei for that particular geometrical arrangement. The potential energy surface therefore represents the energy of the system as a function of the nuclear positions.

1.2.2 Adiabatic Approximation

We assume that the reaction occurs on a single potential energy surface and that coupling between different electronic states does not occur. The adiabatic approximation expands the total molecular wave function as a linear combination of products summed over all electronic states[39]

$$\Psi(R,r) = \sum_i \chi_i(R)\Phi_i(R,r) \tag{1.6}$$

where $\chi_i(R)$ are solutions of the nuclear Schrödinger equation and $\Phi_i(R,r)$ are solutions of the electronic Schrödinger equation.

Integration of Equation 1.6 with respect to the electronic coordinates yields[39]

$$\left[T_n + U_j(R) + E\right]\chi_i(R) + \sum_i \lambda_{ij}(R)\chi_i(R) = 0 \tag{1.7}$$

where $U_j(R)$ is the potential energy function for state j and λ_{ij} are coupling terms. Coupling terms are usually only important between a small number of states. The adiabatic approximation states that the coupling terms between different electronic states are zero. Therefore, only one electronic state is involved, and the nuclear wave equation is[39]

$$\left[T_n + U_j(R)\right]\chi(R) = E\chi(R) \tag{1.8}$$

1.3 Quasiclassical Trajectories

Classical trajectories are solved by simultaneously numerically integrating Hamilton's equations of motion[40]

$$\frac{\partial H}{\partial p_i} = \frac{dq_i}{dt} \tag{1.9}$$

$$\frac{\partial H}{\partial q_i} = -\frac{dp_i}{dt} \tag{1.10}$$

where H is the Hamiltonian function (total energy), p_i is the generalized momentum, q_i is the generalized position, and t is time. We specify the initial velocities and positions of the atoms for the trajectory calculation using Monte Carlo methods, and use of the

equations above in combination with a potential energy surface allows us to propagate the motion of the atoms in a chemical reaction.

In traditional classical dynamics, an analytical potential energy surface that describes the system potential energy as a function of the atomic coordinates is involved in the solution of the equations of motion. In direct dynamics, trajectories are integrated 'on the fly', i.e. the time-independent electronic Schrödinger equation is solved at each numerical integration step to obtain the forces acting on the nuclei as they progress from reactants to products.[40] In the most common implementations of direct dynamics, the wave function is optimized at each integration step of the trajectory.

When calculating quasiclassical trajectories, the initial vibrational and rotational energies are commonly chosen to correspond to known quantum mechanical energy levels.[41] Quasiclassical trajectories are advantageous because they are computationally inexpensive and they allow a wide range of dynamics properties to be studied. Trajectories calculations serve two main purposes: to investigate the features of the dynamics, and to account for observed behavior or to anticipate experimental results.[42] Trajectory calculations can be divided in three separate steps: generation of initial conditions, trajectory propagation, and analysis.

1.3.1 Initial Conditions

When calculating trajectories, some initial conditions need to be assigned. We must choose the impact parameter, which is the closest distance between two reactant species if they travel at their initial velocity and with no outside forces acting on them. We must specify the initial velocities (or momenta) of each reactant atom and the atom's relative positions. We must also assign the initial translational energy and the orientation between the colliding species.

1.3.2 Equations of Motion

The classical equations of motion are integrated to simulate collisions after choosing initial conditions. As stated previously, trajectories are solved by numerically integrating Hamilton's equations (Equations 1.9 and 1.10) at each time step. The

integration step must be small enough that total energy and momentum are conserved during the trajectories, but large enough that the calculations are affordable.

1.3.3 Analysis of Products

In order to obtain a complete coverage of the reaction space, several trajectories must be calculated for each set of reactants' energies, at least 1000 unique (different initial conditions) trajectories.

Total Cross Section

The total (integral) cross section is defined by the equation[42]

$$\sigma_r = 2\pi \int_0^{b_{\max}} P(b)\, b\, db \tag{1.11}$$

where σ_r is the cross section, b is the impact parameter, $P(b)$ is the fraction of reactive collisions occurring with impact parameter b, and b_{max} is the maximum impact parameter used. That equation can be approximated to[42]

$$\sigma_r = \pi b_{\max}^2 \frac{N_{react}}{N_{total}} \tag{1.12}$$

where N_{react} is the number of reactive trajectories and N_{total} is the total number of trajectories calculated.

Differential Cross Section

The total cross section is the integral of the differential cross section ($d\sigma_r/d\omega$)[41]

$$\sigma_r = \int_0^{2\pi} \int_0^{\pi} \frac{d\sigma_r}{d\omega} \sin\theta\, d\theta\, d\phi \tag{1.13}$$

$$\frac{d\sigma_r}{d\omega} = \frac{P(b) b}{\sin\theta \left| \frac{d\theta}{db} \right|} \tag{1.14}$$

where $d\omega = \sin\theta\, d\theta\, d\varphi$, ω is the solid angle, θ is the deflection angle, and φ is the azimuthal angle. The differential cross section shows the angular dependence of the reaction cross section with units of area per solid angle.

Scattering Angle

After a collision, the products might scatter in multiple directions. The scattering angle is defined by the equation[43]

$$\cos\theta_c = \frac{V_{ij} \cdot V_R}{|V_{ij}| \cdot |V_R|} \tag{1.15}$$

where θ_c is the scattering angle, V_R is the initial relative velocity vector between reactants and V_{ij} is the relative velocity vector between the center of masses of products.

Relative Products Translational Energy

The relative products translational energy[43] is defined by

$$E'_T = \frac{1}{2}\mu_{ij} V_{ij}^2 \tag{1.16}$$

where μ_{ij} is the reduced mass of products.

Diatomic Rotational Energy

We need to calculate the rotational distribution of the HF product of the reaction to compare with experiment and thus calibrate the accuracy of our calculations. The rotational quantum number (j) is given from the diatomic angular momentum[44]

$$\mathbf{j} = \mathbf{x}' \times \mathbf{p}' \tag{1.17}$$

$$j(j+1)\hbar^2 = \mathbf{j}^2 \tag{1.18}$$

where $\mathbf{j}$ is the angular momentum, $\mathbf{x}'$ is the position, $\mathbf{p}'$ is the linear momentum, and $\hbar$ is Planck's constant.

The rotational energy[44] is

$$E'_{ROT} = B_e(j)(j+1)\hbar - D_e(j)^2(j+1)^2\hbar^2 - \alpha_e\left(\upsilon + \frac{1}{2}\right)j(j+1)\hbar \tag{1.19}$$

where B_e is the rotational constant, D_e is the centrifugal distortion constant, α_e is the vibration-rotation coupling constant, and υ is the vibrational quantum number.

Diatomic Vibrational Energy

The vibrational quantum number can be obtained by first computing the vibrational energy.[44]

$$E'_{VIB} = E'_{INT} - E'_{ROT} \tag{1.20}$$

As we have already calculated the rotational energy, we now need to find the global energy released to the diatom. We interpolate the internuclear distance (r) into the equation of a Morse potential energy surface for the diatomic and add this potential energy to the diatomic kinetic energy obtained from the diatomic momenta.[44]

$$r = \sqrt{\sum_{i=1}^{3} x'^{2}_{i}} \tag{1.21}$$

$$E'_{INT} = D_e\left(1 - e^{\beta(r-r_e)}\right)^2 + \frac{1}{2\mu}\sum_{i=1}^{3} p'^{2}_{i} \tag{1.22}$$

where i=1,2,3 refers to the x,y,z components, x' refers to position, p' refers to the momentum, β is a parameter describing the width of the potential well, r_e is the equilibrium distance, and μ is the reduced mass. The vibrational quantum number is obtained from the anharmonic expression of the vibrational energy[44]

$$E'_{VIB} = \omega_e\left(\upsilon + \frac{1}{2}\right) - \omega_e x_e\left(\upsilon + \frac{1}{2}\right)^2 \tag{1.23}$$

where ω_e is the vibration wavenumber and $\omega_e x_e$ is an anharmonic constant.

Chapter 2 Potential Energy Surface Characterization

2.1 Reaction Energy

Reaction energies for $F + CH_4 \rightarrow HF + CH_3$ and $F + C_2H_6 \rightarrow HF + C_2H_5$ were calculated using several electronic structure methods and basis sets. The methods used include second-order Møller-Plesset perturbation theory (MP2)[45], the Becke Three Parameter Hybrid Functional with the correlation functional of Lee, Yang, and Parr (B3LYP)[46, 47], coupled-cluster theory[48] with single, double, and perturbative triple excitations (CCSD, CCSD(T)), the parameter model 3 (PM3)[49], Austin model 1 (AM1)[50], and the modified symmetrically orthogonalized intermediate neglect of differential overlap method (MSINDO)[51]. For *ab initio* calculations, Dunning's double-, triple-, and quadruple-zeta correlation consistent basis sets augmented with diffuse functions (aug-cc-pVXZ, X=D,T,Q) and Dunning's triple-zeta correlation consistent basis set (cc-pVTZ) were used.[52] The calculated reaction energies were extrapolated to the complete basis set (CBS) limit using a two-point formula. [53]

$$E_{CBS} = \frac{4^3 E_{aug-cc-pVQZ} - 3^3 E_{aug-cc-pVTZ}}{4^3 - 3^3} \tag{2.1}$$

To allow for the calculation of energies with higher levels of theory and larger basis sets, dual-level calculations have been performed. Dual-level calculations use geometries and harmonic frequencies calculated with a lower level of theory/smaller basis set. This permits the energy to be calculated at a higher level when the computational cost of the geometry optimization and/or harmonic frequency calculation is prohibitive. This technique has been employed for most of the CCSD(T) calculations that have been performed.

2.1.1 $F + CH_4 \rightarrow HF + CH_3$

The experimental reaction energy at room temperature (298 K) is -31.4 kcal/mol[54-56]. Here the 0 K estimate of -32.1 kcal/mol[2] will be used to compare with the electronic structure calculations that we have carried out in an attempt to calibrate the

performance of the computational methods. The results of the calculations are shown in Table 2.1.

Zero-point corrected reaction energies calculated using MP2 theory show a trend of decreasing energy with increasing basis set size. For instance, MP2/aug-cc-pVDZ calculations yielded a reaction energy 3.15 kcal/mol below the experimental value, and MP2/aug-cc-pVTZ calculations predict a reaction energy 4.56 kcal/mol more exothermic than experiment. When the complete basis set estimate is calculated using these MP2 energies, the reaction energy found is over 6 kcal/mol below the experimental value. Although larger basis sets should improve the agreement with experiment, these results indicate that MP2 theory is not a very accurate method for this reaction because increasing the basis set does not produce a closer match with experiment. Therefore, the agreement of MP2/aug-cc-pVDZ calculations with experiments is a fortuitous counterbalancing of the errors of MP2, which tends to overestimate the reaction energy, and a low basis set (i.e. aug-cc-pVDZ), which tends to underestimate the reaction energy. When the reaction energy is calculated with diffuse functions removed, using the cc-pVTZ basis set, the reaction energy comes within 2.5 kcal/mol of the experimental values. The difference of the MP2/cc-pVTZ and MP2/aug-cc-pVTZ zero-point corrected reaction energies is about 3 kcal/mol, indicating that omission of diffuse functions in the basis set will result in inaccurate energies for the $F + CH_4 \rightarrow HF + CH_3$ reaction.

B3LYP calculations yield reaction energies within 1 kcal/mol of the experimental value when aug-cc-pVDZ and aug-cc-pVTZ basis sets are used. The energies for these basis sets are actually quite close to each other with a difference of about 0.1 kcal/mol. When diffuse functions are removed from the aug-cc-pVTZ basis set the reaction energy increases by 2 kcal/mol. Seen here as well as with MP2 theory, the removal of diffuse functions yields more positive, less accurate reaction energies. Therefore, it can be concluded that diffuse functions in the basis set are required to obtain accurate predictions of the reaction energy. Roberto-Neto *et al*.[28] concluded that the importance of diffuse functions is mainly related to the ionic character of the fluorine atom for which the electron affinity is more accurately computed using diffuse functions.

Reaction energies calculated with the CCSD method and aug-cc-pVDZ and aug-cc-pVTZ basis sets are within 1 kcal/mol of each other. The energy calculated using the

aug-cc-pVDZ basis set is about 2.4 kcal/mol higher than the experimental energy, while the aug-cc-pVTZ energy reduces the difference to 1.6 kcal/mol. Removing diffuse functions from the aug-cc-pVTZ basis set yields a reaction energy that is 3.7 kcal/mol above the experimental value.

The reaction energy at the CCSD(T) level was calculated with various basis sets using MP2/aug-cc-pVDZ geometries and harmonic frequencies. The CCSD(T) reaction energy was found to decrease as the size of the basis set was increased, which follows the trend mentioned above for the other *ab initio* calculations. Calculations performed with the aug-cc-pVQZ basis set yielded reaction energy within 0.3 kcal/mol of the experimental value. The complete basis set extrapolation of the CCSD(T) energies was found to be about 1.0 kcal/mol lower than the experimental value (0.5 kcal/mol considering the experimental error bar), which is the level of accuracy expected for this method.

CCSD(T) reaction energies were also calculated using geometries and harmonic frequencies calculated with MP2/aug-cc-pVTZ, CCSD/aug-cc-pVTZ, and CCSD(T)/aug-cc-pVDZ. Results similar to those of MP2/aug-cc-pVDZ were found for each of these methods and basis sets. Quantitatively, the nonzero-point corrected CCSD(T)/CBS reaction energies mentioned above are within 0.1 kcal/mol of each other. These results validate the use of dual-level calculations in this work, as the geometry of reactants and products seems to be well captured by a variety of methods. The results also suggest that it is more important to select an accurate method to calculate the energies than to carry out the geometry optimizations and harmonic frequencies calculation.

The semiempirical Hamiltonians PM3, AM1, and MSINDO were used to calculate the reaction energy. Both unrestricted (U) and restricted open-shell (RO) wave functions have been used. Reaction energies calculated with AM1 were found to be 25 kcal/mol below the experimental value. PM3 reaction energies were found to be higher than AM1, yet still 10.7 – 13.1 kcal/mol below the experimental value. MSINDO yielded the closest energies being 2.5 – 5.1 kcal/mol below the experimental value. For all of the semiempirical Hamiltonians, energies calculated with unrestricted wave functions were slightly lower (at most 2 kcal/mol) than those calculated with restricted open-shell wave functions.

Method	Barrier (ZPE-corrected)	Barrier (classical)	Reaction energy (ZPE-corrected)	Reaction energy (Classical)
MP2/aug-cc-pVDZ	1.46	3.44	-35.25	-31.78
MP2/aug-cc-pVTZ	1.52	3.45	-36.66	-33.03
MP2/aug-cc-pVQZ//MP2/aug-cc-pVTZ	1.44	3.39	-37.61	-33.99
MP2/CBS//MP2/aug-cc-pVTZ	1.38	3.35	-38.31	-34.69
MP2/cc-pVTZ	2.35	4.47	-33.92	-30.40
B3LYP/aug-cc-pVDZ			-31.57	-28.23
B3LYP/aug-cc-pVTZ			-31.68	-28.18
B3LYP/cc-pVTZ			-29.33	-25.81
CCSD/aug-cc-pVDZ	-0.01	1.30	-29.70	-26.26
CCSD/aug-cc-pVTZ			-30.49	-26.92
CCSD/cc-pVTZ	1.28	3.05	-28.38	-24.89
CCSD(T)/aug-cc-pVDZ//MP2/aug-cc-pVDZ	-2.30	-0.32	-30.10	-26.63
CCSD(T)/aug-cc-pVTZ//MP2/aug-cc-pVDZ	-2.30	-0.31	-31.40	-27.93
CCSD(T)/aug-cc-pVQZ//MP2/aug-cc-pVDZ	-2.42	-0.44	-32.40	-28.94
CCSD(T)/CBS//MP2/aug-cc-pVDZ	-2.51	-0.53	-33.13	-29.68
CCSD(T)/aug-cc-pVDZ//MP2/aug-cc-pVTZ	-2.21	-0.26	-30.28	-26.65
CCSD(T)/aug-cc-pVTZ//MP2/aug-cc-pVTZ	-2.19	-0.24	-31.53	-27.91
CCSD(T)/aug-cc-pVQZ//MP2/aug-cc-pVTZ	-2.31	-0.36	-32.53	-28.90
CCSD(T)/CBS//MP2/aug-cc-pVTZ	-2.40	-0.45	-33.26	-29.62
CCSD(T)/aug-cc-pVDZ//CCSD/aug-cc-pVTZ			-30.20	-26.63
CCSD(T)/aug-cc-pVTZ//CCSD/aug-cc-pVTZ			-31.48	-27.91
CCSD(T)/aug-cc-pVQZ//CCSD/aug-cc-pVTZ			-32.36	-28.92
CCSD(T)/CBS//CCSD/aug-cc-pVTZ			-33.00	-29.66
CCSD(T)/aug-cc-pVDZ	0.24	0.89	-30.09	-26.64
CCSD(T)/aug-cc-pVTZ//CCSD(T)/aug-cc-pVDZ			-31.36	-27.92
CCSD(T)/aug-cc-pVQZ//CCSD(T)/aug-cc-pVDZ			-32.36	-28.92
CCSD(T)/CBS//CCSD(T)/aug-cc-pVDZ			-33.09	-29.65
CCSD(T)/aug-cc-pVTZ			-31.49	-27.91
ROPM3	-3.08	0.64	-42.77	-38.85
UPM3	-5.43	-1.86	-44.54	-40.66
ROAM1	7.53	11.02	-56.61	-53.13
UAM1	4.55	7.97	-57.02	-54.44
ROMSINDO	7.05	10.15	-34.57	-30.07
UMSINDO	2.65	3.85	-36.50	-32.70
Exp[2]			-32.1±0.5	
Exp[54]			-31.4±0.3	
Exp[56]			-31.4±0.2	
Exp[55]			-31.4±0.9	

Table 2.1. Reaction energies and reaction barriers for the reaction $F + CH_4 \rightarrow HF + CH_3$. Units are kcal/mol.

In summary, for all first-principles methods used, the reaction energy decreases as the size of the basis set is increased. When diffuse functions are removed from the aug-cc-pVTZ basis set, the reaction energies become about 2 kcal/mol less negative than when diffuse functions were included. The most chemically-accurate results are produced with B3LYP/aug-cc-pVDZ, B3LYP/aug-cc-pVTZ, and dual-level CCSD(T)/aug-cc-pVTZ regardless of the method used to calculate geometries and harmonic frequencies. Our best calculations, CCSD(T)/CBS, are within 1 kcal/mol of the experimental reaction energy.

2.1.2 $F + C_2H_6 \rightarrow HF + C_2H_5$

The $F + C_2H_6 \rightarrow HF + C_2H_5$ reaction is more exothermic than the homologue reaction described above. The lower reaction energy for this reaction can be attributed to the C_2H_5 radical being more stable than the CH_3 radical. More energy is required to break the C-H bond in CH_4 and form the CH_3 radical than is needed to break the C-H bond in C_2H_6. Here we note a discrepancy among the various experimental values available. The reaction energy obtained from the enthalpies of formation of the reactant and product species reported in the Computational Chemistry Comparison and Benchmark Database[2] (CCCBDB) is over 3 kcal/mol more negative than that provided by the rest of the sources consulted here. This is attributed to an incorrect enthalpy of formation for the ethyl radical. The enthalpy of formation is about 120 kJ/mol for three of the sources. However, for the CCCBDB the enthalpy of formation is 107±6 kJ/mol; even considering the uncertainty, the enthalpies of formation do not overlap. It is concluded that the enthalpy of formation of the ethyl radical at 0K should be revised in the CCCBDB database. Therefore, in the following comparison with experiment we will leave aside the CCCBDB value. The results of the calculations are shown in Table 2.2.

Calculations performed using the MP2 level of theory yield reaction energies below the experimental value. MP2/aug-cc-pVDZ reaction energies are 2.1 – 2.7 kcal/mol below the experimental values. As the size of the basis set is increased the reaction energy decreases. The MP2/CBS reaction energy is found to be 5.6 – 6.2 kcal/mol below the experimental values. Increasing the size of the basis set should yield

a more accurate reaction energy, bringing the calculated value closer to those found experimentally. However, for MP2 this is not the case, and the calculated reaction energy is found to be farther away from the experimental values as the size of the basis set is increased; therefore MP2 theory is not best for use with this reaction. These results are analogous to those described previously for $F + CH_4 \rightarrow HF + CH_3$.

B3LYP/aug-cc-pVDZ and B3LYP/aug-cc-pVTZ calculations yield similar reaction energies with about a 0.3 kcal/mol difference. These energies are 0.4 – 1.3 kcal/mol lower than the experimental values. When diffuse functions are excluded and calculations performed with the cc-pVTZ basis set, the reaction energy is 1.6 kcal/mol higher than the reaction energy calculated with the aug-cc-pVTZ basis set.

Reaction energies calculated using the CCSD method exhibit a decrease of about 1 kcal/mol when the basis set is increased from aug-cc-pVDZ to aug-cc-pVTZ. These reaction energies are 1.5 – 3.2 kcal/mol higher than the experimental values. When the cc-pVTZ basis set is used the reaction energy is about 2 kcal/mol less negative than the corresponding result with the aug-cc-pVTZ basis set.

Using geometries and harmonic frequencies calculated with MP2/aug-cc-pVDZ, reaction energies were calculated using the CCSD(T) method and various basis sets. As the size of the basis set used was increased, the reaction energy decreased. The energies were found to be 0.1 – 2.5 kcal/mol away from the experimental values. Our best calculations, CCSD(T)/CBS, provide reaction energies within 1 kcal/mol of the experiment. As with $F + CH_4$, CCSD(T) yields the most accurate results among the *ab initio* methods employed in this work.

Reaction energies were also calculated using CCSD(T)/aug-cc-pVDZ, CCSD/aug-cc-pVTZ and MP2/aug-cc-pVTZ geometries and frequencies. These values are similar to the reaction energies determined using CCSD(T) with MP2/aug-cc-pVDZ geometries. In fact, for all of the geometries used for CCSD(T) calculations, the reaction energy was found to differ by less 0.2 kcal/mol. This suggests that the level of theory used to calculate the geometries is not as important as the level of theory used to find the energy.

Method/Basis Set	Barrier (ZPE-corrected)	Barrier (classical)	Reaction energy (ZPE-corrected)	Reaction energy (Classical)
MP2/aug-cc-pVDZ	0.16	1.65	-38.01	-34.35
MP2/aug-cc-pVTZ	0.25	1.73	-39.71	-36.00
MP2/aug-cc-pVQZ//MP2/aug-cc-pVTZ	0.23	1.71	-40.75	-37.04
MP2/CBS//MP2/aug-cc-pVTZ	0.22	1.70	-41.51	-37.80
MP2/cc-pVTZ	1.03	2.62	-36.96	-33.34
B3LYP/aug-cc-pVDZ			-36.31	-32.60
B3LYP/aug-cc-pVTZ			-36.63	-32.86
B3LYP/cc-pVTZ			-34.28	-30.50
CCSD/aug-cc-pVDZ	-0.78	-0.20	-32.75	-29.10
CCSD/aug-cc-pVTZ			-33.85	-30.15
CCSD/cc-pVTZ		1.19	-31.69	-28.06
CCSD(T)/aug-cc-pVDZ//MP2/aug-cc-pVDZ	-3.63	-2.14	-33.36	-29.54
CCSD(T)/aug-cc-pVTZ//MP2/aug-cc-pVDZ	-3.50	-2.01	-34.90	-31.25
CCSD(T)/aug-cc-pVQZ//MP2/aug-cc-pVDZ			-35.99	-32.34
CCSD(T)/CBS//MP2/aug-cc-pVDZ			-36.79	-33.14
CCSD(T)/aug-cc-pVDZ//MP2/aug-cc-pVTZ	-3.63	-2.15	-33.26	-29.55
CCSD(T)/aug-cc-pVTZ//MP2/aug-cc-pVTZ	-3.49	-2.01	-34.94	-31.23
CCSD(T)/aug-cc-pVQZ//MP2/aug-cc-pVTZ	-3.57	-2.09	-36.05	-32.34
CCSD(T)/CBS//MP2/aug-cc-pVTZ	-3.63	-2.15	-36.86	-33.15
CCSD(T)/aug-cc-pVDZ//CCSD/aug-cc-pVTZ			-33.27	-29.57
CCSD(T)/aug-cc-pVTZ//CCSD/aug-cc-pVTZ			-34.94	-31.23
CCSD(T)/aug-cc-pVQZ//CCSD/aug-cc-pVTZ			-36.06	-32.35
CCSD(T)/CBS//CCSD/aug-cc-pVTZ			-36.88	-33.17
CCSD(T)/aug-cc-pVDZ			-33.20	-29.55
CCSD(T)/aug-cc-pVTZ//CCSD(T)/aug-cc-pVDZ			-34.90	-31.25
CCSD(T)/aug-cc-pVQZ//CCSD(T)/aug-cc-pVDZ			-36.01	-32.36
CCSD(T)/CBS//CCSD(T)/aug-cc-pVDZ			-36.98	-33.17
ROPM3	-0.19	-0.07	-50.80	-47.22
UPM3	-8.00	-4.24	-52.31	-48.98
ROAM1	-0.46	-0.53	-61.85	-58.98
UAM1	3.05	6.61	-62.89	-60.27
ROMSINDO	3.11	6.21	-44.10	-40.60
UMSINDO	1.28	1.98	-46.10	-42.80
Exp[2]			-39.1±1.4	
Exp[54]			-35.9±0.5	
Exp[56]			-35.3±0.4	
Exp[55]			-35.3±0.4	

Table 2.2. Reaction energies and reaction barriers for the reaction $F + C_2H_6 \rightarrow HF + C_2H_5$. Units are kcal/mol.

Reaction energies were calculated using the semiempirical Hamiltonians PM3, AM1, and MSINDO. Both unrestricted and restricted open shell functions were considered. All of the semiempirical reaction energies calculated are lower than the experimental values with the lowest, UAM1, being about 27 kcal/mol below. This contrasts the *ab initio* values, which tended to be in closer agreement with experiment. PM3 values were about 10 kcal/mol higher than AM1 and MSINDO values were about 6 kcal/mol above PM3. For all of the semiempirical Hamiltonians, energies calculated with unrestricted wave functions were slightly more negative than those calculated with restricted open-shell wave functions.

In summary, for all *ab initio* methods used here, the reaction energy decreases as the size of the basis set is increased. When diffuse functions are removed from the basis set, less accurate reaction energy is obtained. The most chemically accurate results are produced with B3LYP/aug-cc-pVDZ, B3LYP/aug-cc-pVTZ, and dual-level CCSD(T)/aug-cc-pVTZ calculations regardless of the level at which the geometries are calculated. All of these methods/basis sets give reaction energies that are less than 1 kcal/mol away from the experimental values. Our best calculations, CCSD(T)/CBS, provide reaction energies also within 1 kcal/mol of experiments when the experimental error is included.

All of the trends observed for the $F + C_2H_6 \rightarrow HF + C_2H_5$ reaction are analogous to those seen for the $F + CH_4 \rightarrow HF + CH_3$ reaction. This result provides a useful tool to predict the performance of these methods in reactions of fluorine radicals with longer-chain saturated hydrocarbons.

2.2 Reaction Barrier

Reaction barriers were calculated using MP2, B3LYP, CCSD, and CCSD(T) levels of theory. MSINDO, AM1, and PM3 semiempirical Hamiltonians were also used. The values of the reaction barriers can be seen in Tables 2.1 and 2.2 in the previous section. Key geometric parameters of the transition states are shown in Tables 2.3 and 2.4.

2.2.1 $F + CH_4 \rightarrow HF + CH_3$

Calculations performed with MP2 theory yielded very small but positive reaction barriers. Calculations using basis sets augmented with diffuse functions had reaction barriers in the range 1.38 – 1.52 kcal/mol, with the lowest reaction barrier, 1.38 kcal/mol, belonging to the MP2/CBS//MP2/aug-cc-pVTZ results. When diffuse functions were removed from the aug-cc-pVTZ basis set, the barrier was to found to be about 1 kcal/mol higher, 2.35 kcal/mol for MP2/cc-pVTZ.

Figure 2.1 shows a schematic of the transition state calculated with MP2/aug-cc-pVTZ. The structure clearly shows that the breaking and forming bonds are collinear with this level of theory. Therefore, the symmetry of the transition state is C_{3v} at the MP2/aug-cc-pVTZ level. The F-H, C-H, C-H' bond lengths of the transition state are similar for MP2 calculations with the aug-cc-pVDZ, aug-cc-pVTZ, and cc-pVTZ basis sets. (F-H and C-H are the forming and breaking bonds, respectively, and C-H' refers to the inactive bond) The C-H distance at the transition state is only slightly longer than in methane (a 3.5 % increase), but the H-F distance is substantially longer than the internuclear distance in the HF product (a 55 % difference). These results mean that the transition state is reactants-like, as expected in a very exothermic reaction. The H-C-H' angles are ~107°.

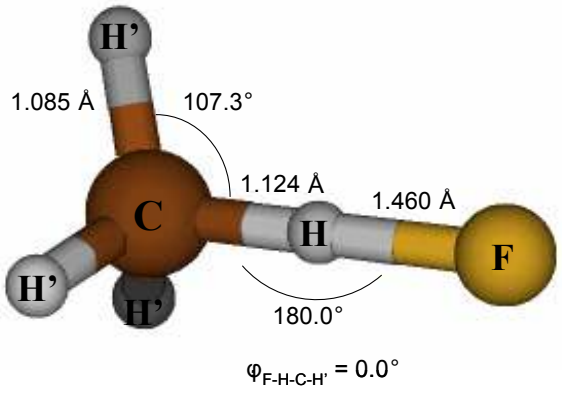

Figure 2.1. F-H-CH_3 transition state calculated with MP2/aug-cc-pVTZ.

With CCSD/aug-cc-pVDZ, a negative zero-point corrected reaction barrier of -0.01 kcal/mol is found. The barrier increases to 1.28 kcal/mol in calculations using the

cc-pVTZ basis set. The F-H bond length is ~0.1 Å longer with the aug-cc-pVDZ basis set than with the cc-pVTZ basis set. In addition, the aug-cc-pVDZ calculations predict that the transition state does not have a collinear F-H-C configuration.

MP2/aug-cc-pVDZ geometries and harmonic frequencies were used to calculate reaction barriers with the CCSD(T) method and multiple basis sets. These barriers were found to be close together, -2.30 to -2.51 kcal/mol. The lowest barrier was found when the CBS extrapolation procedure was performed. Using MP2/aug-cc-pVTZ geometries and harmonic frequencies, the same CCSD(T) calculations were done. Results similar to the MP2/aug-cc-pVDZ calculations were found, with the range of the barriers being -2.21 to -2.40 kcal/mol. There is little difference between the results found with the MP2/aug-cc-pVDZ geometries and the MP2/aug-cc-pVTZ geometries.

The barrier was also located using the CCSD(T)/aug-cc-pVDZ combination. The G03 suite of programs[57] does not include analytical first or second derivatives of the energy, so this geometry optimization required many single-point evaluations to calculate derivatives numerically. With this method/basis set, the barrier was found to be 0.24 kcal/mol. This is about 2 kcal/mol higher than the barrier estimated using CCSD(T)//MP2 dual-level calculations, and indicates that unlike the reaction energy, the reaction barrier is dependent on the level of theory employed to obtain the geometry. These results can also be verified in the transition-state geometries of Table 2.3. The table shows that the F-H internuclear distance at the CCSD(T) level is about 0.2 Å longer than those found with MP2 theory. It also is about 0.1 Å longer than the CCSD/aug-cc-pVDZ geometry.

Of particular interest is the F-H-C angle. Most other calculations show this angle to be 180° while CCSD(T)/aug-cc-pVDZ shows an angle of 157.9°. To investigate this, the dependence of the barrier on the F-H-C angle has been calculated. As seen in Figure 2.2 the potential energy surface is isotropic near the saddle point.[31] As the angle of the saddle point is scanned from 130° to 180° (with the other geometries held fixed to the transition state geometry) no significant change is seen in the energy.

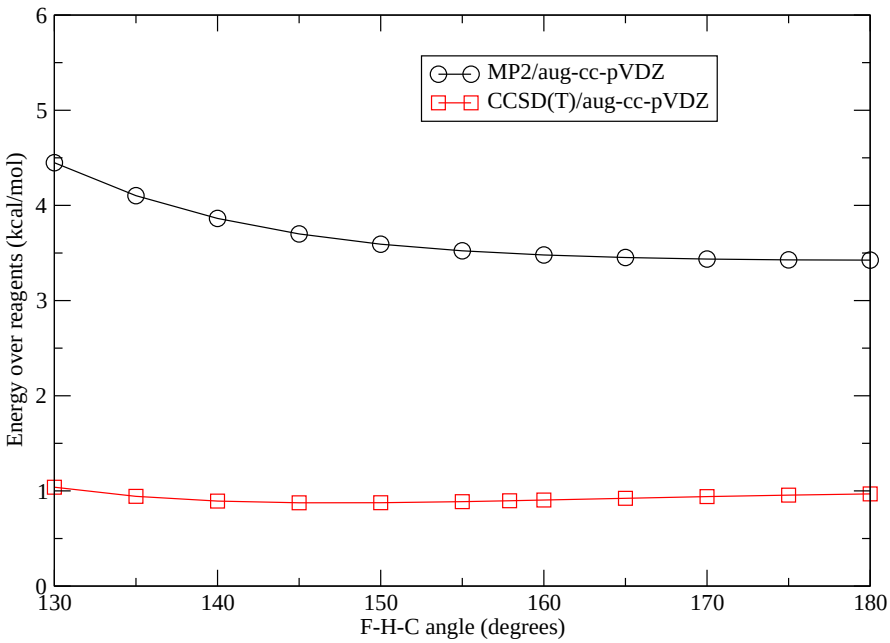

Figure 2.2. Variation of energy with the F-H-C angle for the F + CH_4 → HF + CH_3 reaction at the transition state.

For the semiempirical Hamiltonians, the only method that yielded a negative barrier was PM3, with a restricted open shell barrier of -3.08 kcal/mol and an unrestricted barrier of -5.43 kcal/mol. ROAM1 gave a barrier of 7.53 kcal/mol and UAM1 a barrier of 4.55 kcal/mol. ROMSINDO generated a barrier of 7.05 kcal/mol and UMSINDO a barrier of 2.65 kcal/mol. For all semiempirical Hamiltonians used the unrestricted barrier is lower, and this matches the trend observed in the reaction energies. The semiempirical F-H internuclear distances range in length from 1.126Å to 1.383Å. For each semiempirical method the restricted open shell internuclear distance at the transition state is shorter than the unrestricted length. The C-H lengths range from 1.131Å to 1.176Å. For PM3 and AM1 the unrestricted and restricted open shell C-H lengths are the same, however, for MSINDO we note a 0.05Å difference between the references, with UMSINDO predicting a shorter length. This is accompanied by a notably longer F-H internuclear distance. In other words, while the geometries predicted by unrestricted and restricted open shell references are similar in AM1 and PM3, for UMSINDO estimates a much 'earlier' transition state than ROMSINDO. All of the semiempirical methods show a collinear F-H-C angle.

The calculated reaction barrier can be compared with the activation energy from kinetics experiments. While a direct comparison cannot be made, the activation energy lets us know if the reaction barrier is roughly correct. Persky reports an activation energy of 0.43 kcal/mol for this reaction.[19] This agrees with the values that we have calculated that indicate that this reaction has a small barrier.

	rF-H	rC-H	angF-H-C	angH-C-H'	rC-H'
MP2/aug-cc-pVDZ	1.467	1.136	180.0	107.1	1.096
MP2/aug-cc-pVTZ	1.460	1.124	180.0	107.3	1.084
MP2/cc-pVTZ	1.431	1.126	180.0	107.2	1.084
CCSD/aug-cc-pVDZ	1.563	1.129	179.9	107.6	1.100
CCSD/cc-pVTZ	1.468	1.126	180.0	107.3	1.086
CCSD(T)/aug-cc-pVDZ	1.647	1.123	157.9	107.4	1.102
ROMSINDO	1.126	1.181	180.0	106.9	1.076
UMSINDO	1.285	1.131	180.0	108.0	1.076
UPM3	1.382	1.176	180.0	105.6	1.082
ROPM3 GAMESS	1.339	1.171	180.0	105.8	1.083
UAM1	1.342	1.211	180.0	105.9	1.106
ROAM1 GAMESS	1.292	1.214	179.6	105.9	1.106

Table 2.3. Relevant geometrical parameters of the transition state of the $F + CH_4 \rightarrow HF + CH_3$ reaction. Distances are in Angstroms, and angles in degrees.

Calculations using the B3LYP method and the aug-cc-pVDZ and aug-cc-pVTZ basis sets failed to locate the transition state. Scans of the reaction coordinate show that the reaction proceeds continuously downhill from reactants to products. This is in disagreement with the results of higher accuracy *ab initio* methods. Therefore, while B3LYP predicts reaction energies in great agreement with experiments, this method fails to provide an accurate description of the transition state region.

2.2.2 $F + C_2H_6 \rightarrow HF + C_2H_5$

Reaction barriers calculated using MP2 theory and basis sets including diffuse functions yielded similar results. The zero-point reaction barrier at the MP2/CBS level is 0.22 kcal/mol. Removing diffuse functions from the aug-cc-pVTZ basis set increased the barrier by 0.78 kcal/mol. In contrast with the results of the $F + CH_4 \rightarrow HF + CH_3$ transition state, MP2 predicts that the transition state of $F + C_2H_6 \rightarrow HF + C_2H_5$ is not collinear. There are not large differences in the MP2 transition state geometries using

different basis sets, except for a notable difference in the F-H-C-C dihedral angles. (Here, H is the atom being abstracted.)

To investigate these differences, a scan of the F-H-C-C dihedral from 0° – 360° was performed using MP2/aug-cc-pVDZ as shown in Figure 2.3. The scan (with the rest of the geometry held fixed at the transition state) shows a variance of less than 0.2 kcal/mol for the energy. This indicates that the energy is not strongly dependent on the dihedral angle. The insensitivity of the potential energy to the F-H-C-C dihedral angle seems to be rooted in the very 'early' character of the transition state. The fact that the F atom is far away from the C_2H_6 molecule at the transition state does not allow for the expected repulsions that regularly appear when the system explores geometries removed from those of the minimum energy reaction path.

We have also performed a scan of the F-H-C angle. The angle of the saddle point was scanned from 130° to 180° with the other geometries held fixed to the transition state geometry. Figure 2.4 shows the result of this scan. No significant change is observed in the energy of the CCSD/aug-cc-pVDZ calculations.

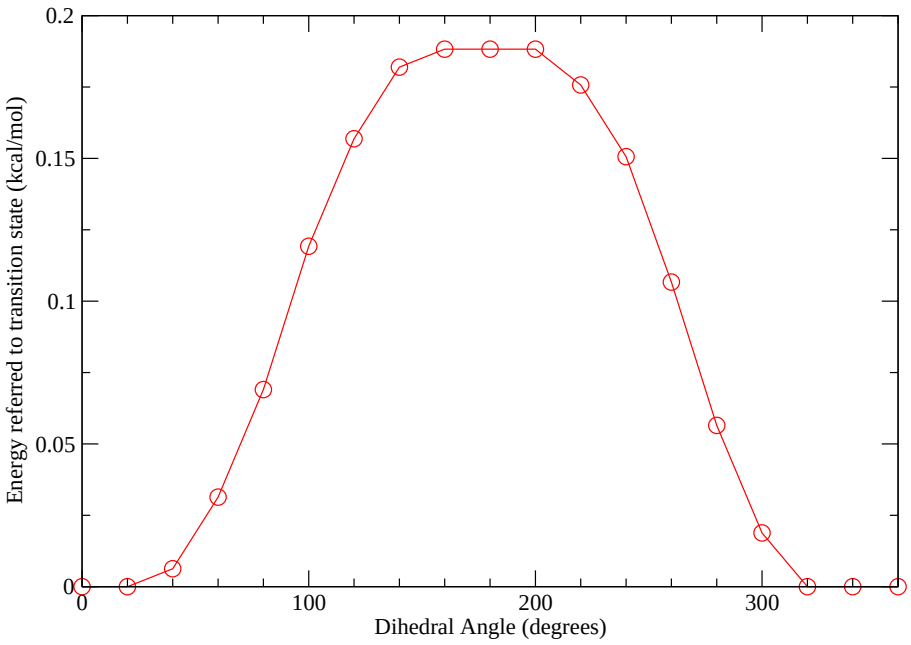

Figure 2.3. Scan of the C-C-H-F dihedral angle of the transition state F-H-C_2H_5 using MP2/aug-cc-pVDZ.

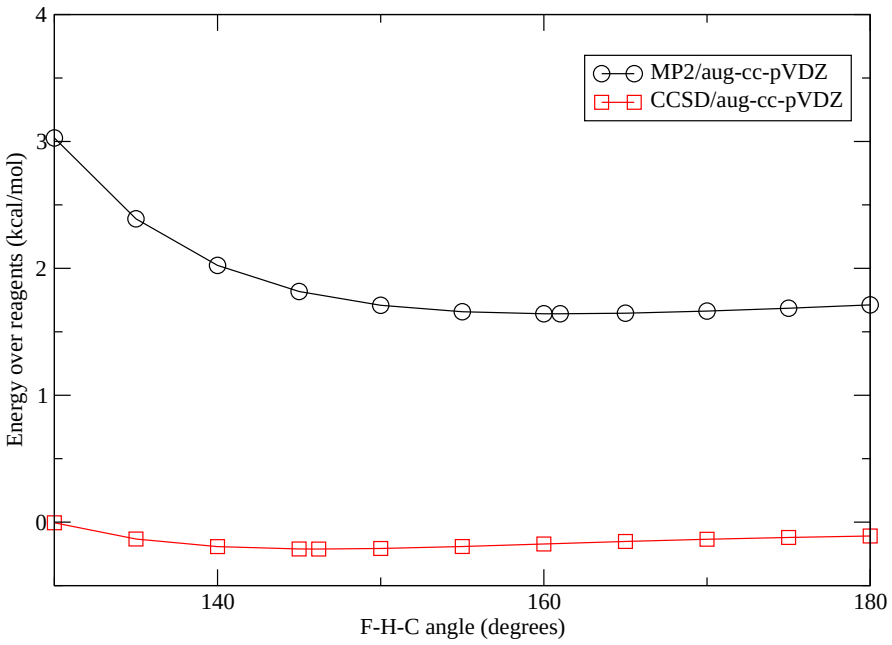

Figure 2.4. Variation of energy with the F-H-C angle for the F + C_2H_6 → HF + C_2H_5 at the transition state.

CCSD/aug-cc-pVDZ yields a zero-point corrected reaction barrier of -0.78 kcal/mol. The classical barrier for CCSD/cc-pVTZ was found to be 1.19 kcal/mol, 1.39 kcal/mol above the classical barrier for CCSD/aug-cc-pVDZ. The CCSD/aug-cc-pVDZ geometry has a F-H bond that is about 0.2 Å longer than the MP2 geometries. Figure 2.5 shows a schematic of the transition state calculated with CCSD/aug-cc-pVDZ. The structure clearly shows that the breaking and forming bonds are not collinear with this level of theory. Since the C-C-F-H dihedral is not 0 or 180°, the symmetry of the transition state is C_1 at the CCSD/aug-cc-pVDZ level. In this discussion, F-H and C-H are the forming and breaking bonds, respectively, and C-H' and C-H'' refer to the inactive bonds on the moiety undergoing hydrogen abstraction.

The reaction barrier was calculated with CCSD(T) theory and multiple basis sets using MP2/aug-cc-pVDZ and MP2/aug-cc-pVTZ geometries and harmonic frequencies. These barriers were found to be -3.49 and -3.63 kcal/mol. These results are more negative than the other *ab initio* calculations. As with the F + CH_4 → HF + CH_3 reaction, the reaction barrier is dependent on the level of theory used to obtain the geometry.

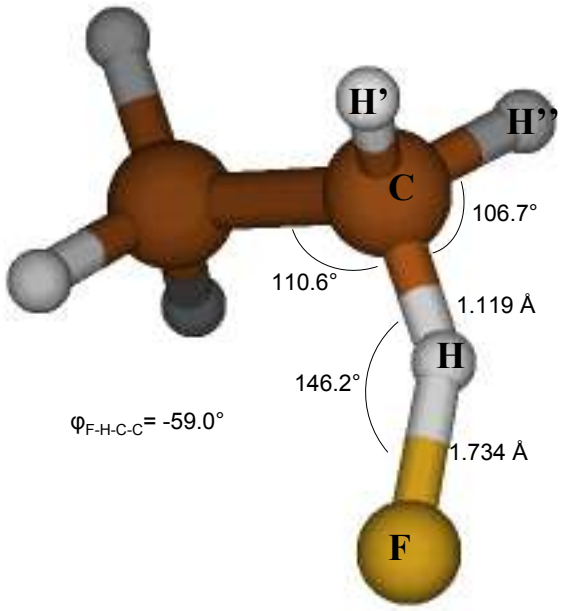

Figure 2.5. F-H-C_2H_5 transition state calculated with CCSD/aug-cc-pVDZ.

In this case, we could not afford to locate the transition state at the CCSD(T) level. However, an estimate of the geometry of the transition state at the CCSD(T) can be obtained from an exploration of the potential energy surface, which will be addressed in the next section.

It is important to note that the amount of discrepancy seen with the semiempirical reaction energies is not observed for the reaction barriers. PM3 calculations using restricted open shell wave functions yield a reaction barrier of -0.19 kcal/mol, within 1 kcal/mol of most of the MP2 and CCSD calculations. However, the PM3 barrier found with unrestricted wave functions is -8.00 kcal/mol, much lower than any of the other calculations. The ROAM1 barrier is similar to the ROPM3 barrier. However, the UAM1 barrier is much higher, ~11 kcal/mol. The ROMSINDO barrier is ~1.8 kcal/mol higher than the UMSINDO barrier. The ROMSINDO barrier is the highest reaction barrier of any calculated.

	rF-H	rC-H	angF-H-C	angH-C-H′	angH-C-C	F-H-C-C dihedral
MP2/aug-cc-pVDZ	1.544	1.130	161.0	105.6	110.2	-22.3
MP2/aug-cc-pVTZ	1.536	1.118	161.1	105.7	110.3	0.0
MP2/cc-pVTZ	1.506	1.120	160.2	105.6	110.2	-0.0
CCSD/aug-cc-pVDZ	1.734	1.119	146.2	106.4	110.6	-59.0
CCSD/cc-pVTZ	1.592	1.114	156.2	105.9	110.5	0.0
ROPM3 GAMESS	2.209	1.101	124.7	107.0	111.5	122.1
UPM3	1.433	1.189	178.3	102.7	110.0	180.0
ROAM1 GAMESS	2.285	1.119	170.5	108.1	110.7	-81.2
UAM1	1.372	1.213	172.2	104.5	108.6	180.0
ROMSINDO	1.173	1.181	169.6	105.9	108.8	-154.1
UMSINDO	1.401	1.128	175.2	107.1	110.2	0.0

Table 2.4. Relevant geometrical parameters of the transition state of the $F + C_2H_6 \rightarrow HF + C_2H_5$ reaction. Distances are in Angstroms, and angles in degrees. H-C-H' angles have been averaged for nonsymmetrical geometries.

The ROPM3 structure has a F-H internuclear distance that is about 0.8 Å longer than the UPM3 structure and about 0.5 Å longer than the CCSD/aug-cc-pVDZ structure. As with PM3, the ROAM1 transition state geometry has an F-H internuclear distance that is much longer than the other methods. In this case, it is about 0.9 Å longer than the UAM1 F-H distance. The ROMSINDO transition state F-H internuclear distance is shorter than that found with any other method. The ROMSINDO distance is about 0.2 Å shorter than the UMSINDO bond. For all semiempirical methods used there is a 0.1 Å variance in the C-H distance with the longest, 1.213 Å, being found with UAM1. The F-H-C angles fall in the range 169.6° - 178.3°, except for ROPM3 which produces an angle of 124.7°.

As with the previous reaction we can make a general comparison with the activation energy obtained from kinetics experiments. The experimental value of 0.36 kcal/mol is slightly smaller than that for $F + CH_4 \rightarrow HF + CH_3$.[36] The calculated reaction barriers also indicate that the $F+C_2H_6 \rightarrow HF + C_2H_5$ reaction has a smaller barrier than the smaller homologue reaction.

2.3 Minimum Energy Reaction Path

The intrinsic reaction coordinate (IRC) calculation follows the reaction path in the forward and reverse directions from the transition state.[58] The reaction is stepped along the minimum energy reaction path towards either products or reactants. The geometry is optimized at this point of the reaction coordinate and then another step is taken along the reaction path.

2.3.1 $F + CH_4 \rightarrow HF + CH_3$

The IRC was calculated using MP2/aug-cc-pVDZ. The plot of energy vs. reaction coordinate (Figure 2.6) shows a slight uphill from reactants to the barrier then a drop towards products. Using the MP2/aug-cc-pVDZ geometries, the energy was calculated with MP2/aug-cc-pVTZ. The plot for MP2/aug-cc-pVTZ is nearly identical to the plot for MP2/aug-cc-pVDZ, with the –TZ plot showing a lower energy in the products range, which is consistent with the lower reaction energy predicted with the larger basis set (Table 2.1). The MP2/aug-cc-pVDZ geometries were also used to calculate a dual-level IRC with energies computed using UAM1. The UAM1 plot shows a much higher barrier that is shifted towards products. The descent towards products is much steeper, yielding a final energy that is over 10 kcal/mol lower than MP2/aug-cc-pVDZ. Dual-level calculations were also performed using UPM3. This plot shows a decrease in energy from reactants, followed by an increase to the reaction barrier, forming a well. The UPM3 barrier is lower than that of methods previously used. The energy resulting from the decrease to products is lower than that of the methods used except for UAM1. Lastly, dual-level calculations were performed using CCSD(T)/aug-cc-pVDZ. The CCSD(T) plot shows a barely visible reaction barrier which corresponds to the calculated barrier of 0.88 kcal/mol. Also CCSD(T) yields the highest reaction energy according to the plot which corresponds to previously mentioned results.

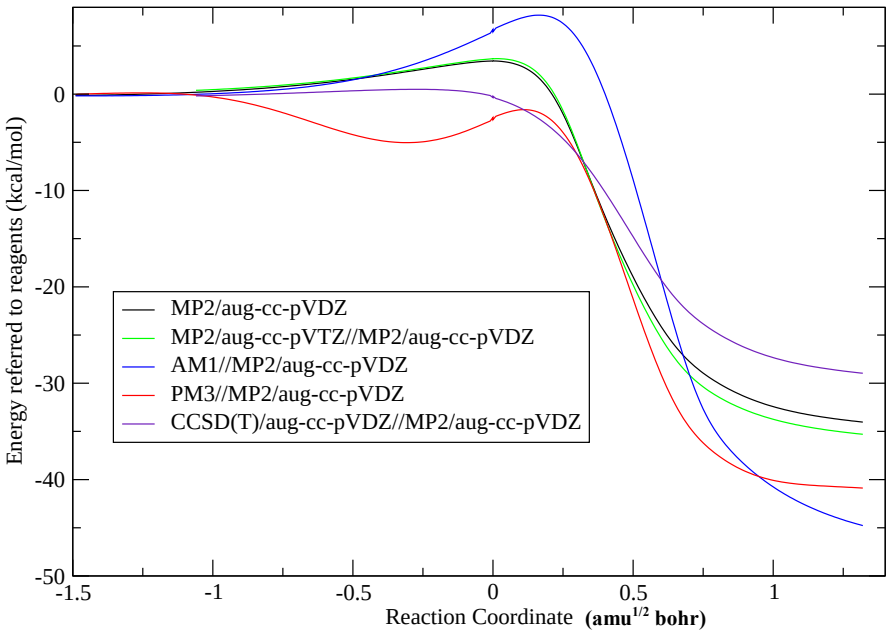

Figure2. 6. Intrinsic reaction coordinate for F + CH_4 → HF + CH_3.

2.3.2 F + C_2H_6 → HF + C_2H_5

The IRC was calculated using MP2/aug-cc-pVDZ. The MP2/aug-cc-pVDZ geometries were then used to calculate the energy using MP2/aug-cc-pVTZ, AM1 U, PM3 U, and CCSD(T)/aug-cc-pVDZ. The results are similar to those of the reaction F + CH_4 → HF + CH_3. One main difference is a lower barrier and more negative reaction energy for all methods. The other major difference that is observed is that unlike the F + CH_4 → HF + CH_3 reaction, the PM3 method yields a reaction energy that is lower than that predicted by AM1. The disagreement between the AM1 reaction energy seen in the IRC and the energy calculated previously can be attributed to the use of MP2/aug-cc-pVDZ optimized geometries. The H-F distance in the MP2 optimized structure is 0.925 Å while AM1 has a distance of 0.826 Å. CCSD(T)/aug-cc-pVDZ shows a continuous downhill slope with no evident barrier. This feature can be observed better in the potential energy surface scan shown in the next section.

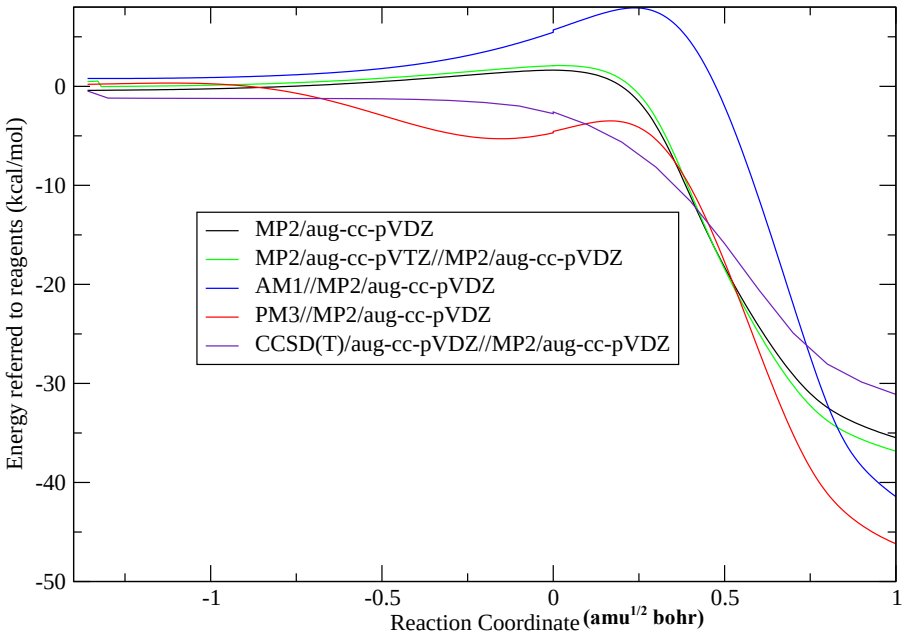

Figure 2.7. Intrinsic reaction coordinate for F + C_2H_6 → HF + C_2H_5

2.4 Potential Energy Surface Scans

2.4.1 F + CH_4 → HF + CH_3

To further investigate the potential energy surface of the F + CH_4 → HF + CH_3 reaction, an energy scan of the breaking and forming bonds is performed. The C-H bond distance is varied from 1.01 Å to 2.72 Å (step size 0.09Å) and the F-H bond distance is varied from 0.70 Å to 2.41 Å (step size 0.09Å) such that a total of 400 points are calculated. The geometry is optimized at each point with the F-H and C-H distances held fixed and the F-H-C angle held fixed at 180°. The energies obtained from these calculations are then plotted as a function of the F-H and C-H internuclear distances to yield the contour plot in Figure 2.8. The plot shows the barrier at a F-H distance of about 1.5 Å and a C-H distance of about 1.1 Å. The minimum energy reaction path can be observed starting in the lower right corner of the plot traveling horizontally to the left then upwards towards the upper left corner. As discussed previously, the scan shows

little variance in the C-H distance when traveling from reactants to the transition state, indicating the reaction's 'early' transition state.

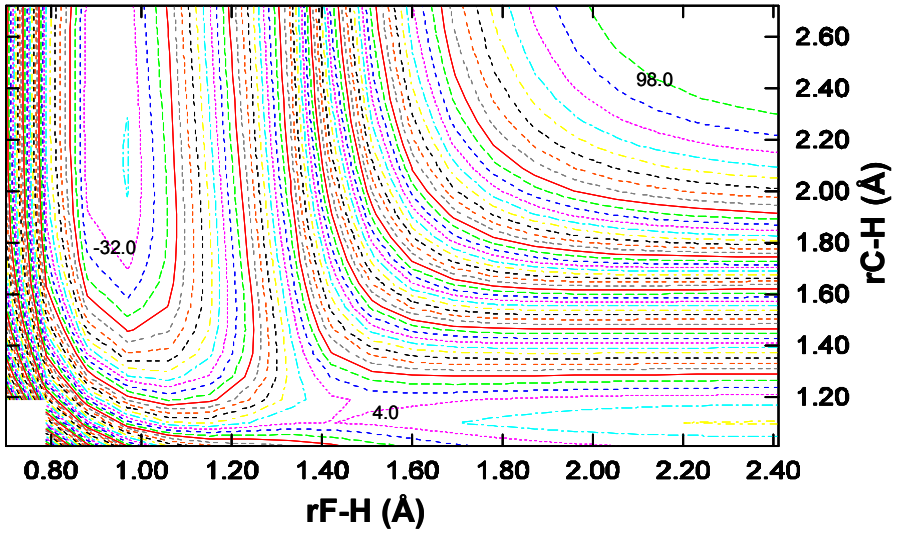

Figure 2.8. Potential energy surface scan of the reaction F + CH_4 → HF + CH_3 using MP2/aug-cc-pVDZ. Energy contours are plotted each 2 kcal/mol.

The MP2/aug-cc-pVDZ geometries are then used to calculate the CCSD(T)/aug-cc-pVDZ energies for the 400 points of the scan. The CCSD(T)//MP2/aug-cc-pVDZ potential energy surface scan is shown in Figure 2.9. As with the MP2/aug-cc-pVDZ plot, the minimum energy reaction path can be seen starting in the lower right corner traveling horizontally to the left then upwards toward the upper left corner. The classical barrier of 0.88 kcal/mol and reaction energy of -26.64 kcal/mol can be observed in the plot.

PM3 energies were also calculated using the MP2/aug-cc-pVDZ geometries. The plot is shown in Figure 2.10. A feature of the PM3 potential energy surface that is not observed by the other methods is a well between the reactants and the transition state. This is a failure of the method. As with the other methods, the minimum energy reaction path can be observed starting the lower right corner and traveling horizontally to the left and upwards to the upper left corner. The classical barrier of -1.86 kcal/mol and the classical reaction energy of -40.66 kcal/mol can be observed in the plot.

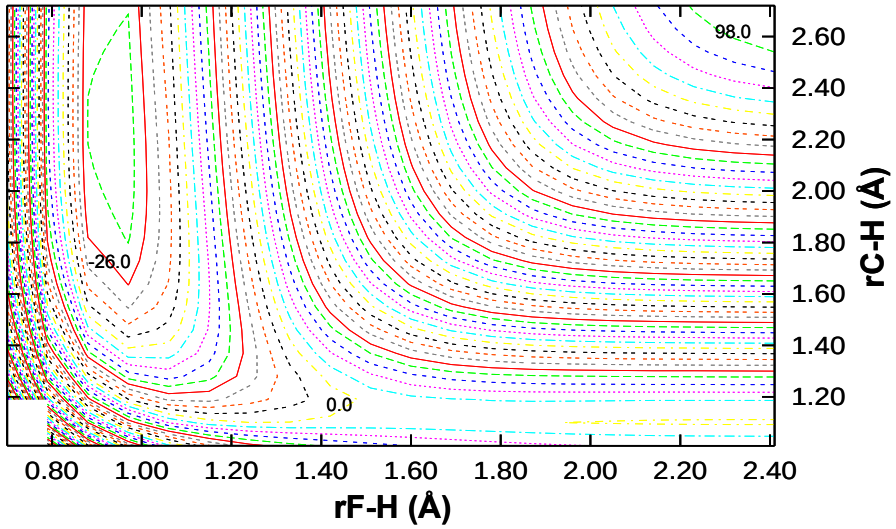

Figure 2.9. Potential energy surface scan of the reaction F + CH_4 → HF + CH_3 using CCSD(T)/aug-cc-pVDZ//MP2/aug-cc-pVDZ. Energy contours are plotted each 2 kcal/mol.

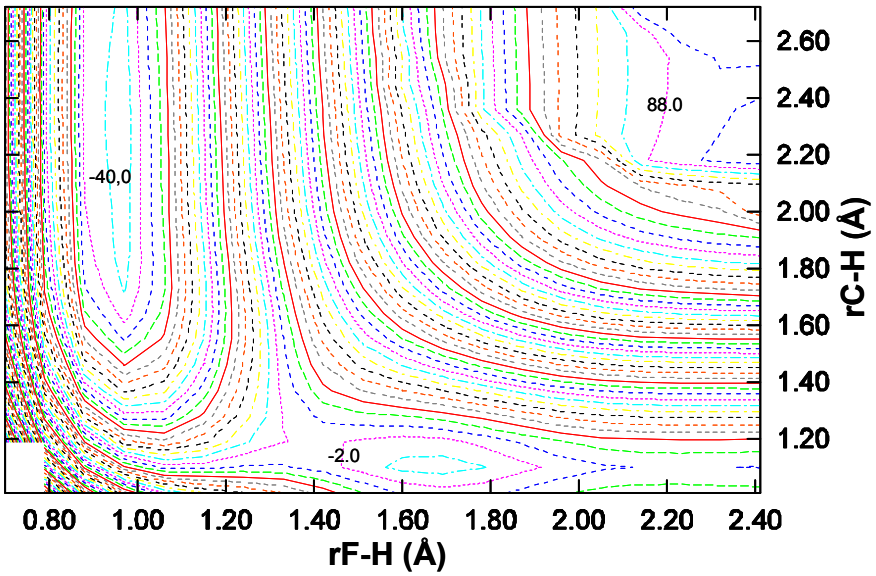

Figure 2.10. Potential energy surface scan of the reaction F + CH_4 → HF + CH_3 using PM3//MP2/aug-cc-pVDZ. Energy contours are plotted each 2 kcal/mol.

2.4.2 $F + C_2H_6 \rightarrow HF + C_2H_5$

Potential energy scans have been completed for the $F + C_2H_6 \rightarrow HF + C_2H_5$ reaction using the same methods as used for $F + CH_4 \rightarrow HF + CH_3$. The C-H bond is scanned from 1.01 Å to 2.72 Å (step size 0.09Å) and the F-H bond is scanned from 0.75 Å to 2.46 Å (step size 0.09Å) yielding a grid of 400 points. Figure 2.11 shows the surface calculated with MP2/aug-cc-pVDZ. The barrier is visible at a F-H bond length of 1.5 Å and a C-H bond length of 1.1 Å, which is consistent with the transition state distances listed in Table 2.4. As with the $F + CH_4 \rightarrow HF + CH_3$ reaction, the minimum energy reaction path is observed starting in the lower right corner moving horizontally to the left and upwards towards the upper left corner.

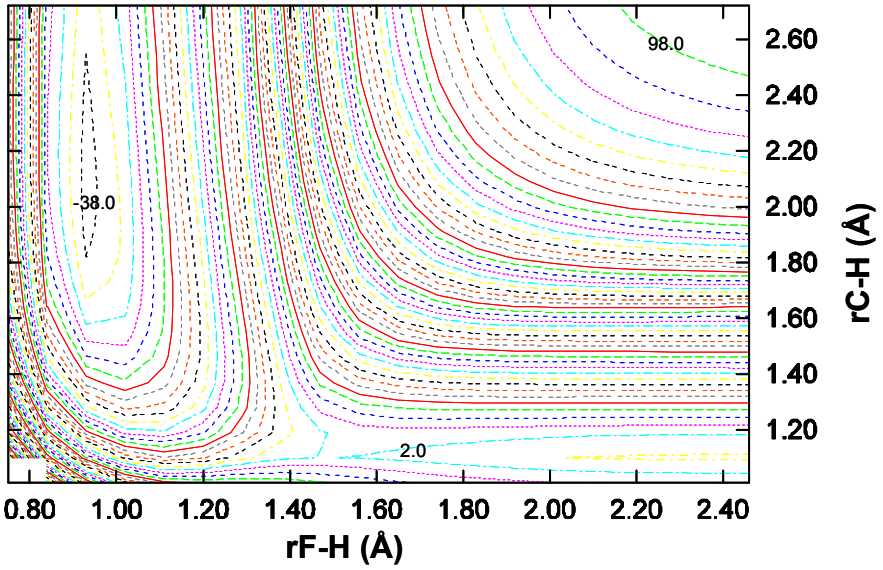

Figure 2.11. Potential energy surface scan for the reaction $F + C_2H_6 \rightarrow HF + C_2H_5$ using MP2/aug-cc-pVDZ. Energy contours are plotted each 2 kcal/mol.

The MP2/aug-cc-pVDZ geometries were then used to calculate the energies with CCSD(T)/aug-cc-pVDZ. Unlike the other potential energy surface scans the CCSD(T) results show no barrier. Instead, the pathway from reactants to products is continuously downhill. This confirms the results of the IRC calculation where no barrier was observed. The minimum energy reaction path is again seen starting in the lower right corner, then proceeding horizontally to the left and upwards to the upper left corner.

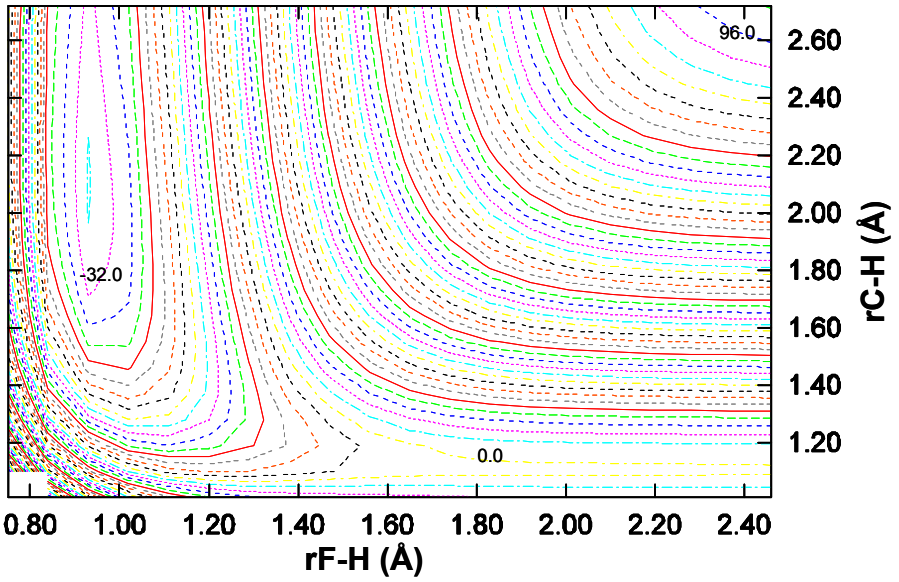

Figure 2.12 . Potential energy surface scan for the reaction F + C_2H_6 → HF + C_2H_5 using CCSD(T)/aug-cc-pVDZ//MP2/aug-cc-pVDZ. Energy contours are plotted each 2 kcal/mol.

The MP2/aug-cc-pVDZ geometries were also used to calculate PM3 energies. As with the F + CH_4 → HF + CH_3 reaction, a well is observed between reactants and the transition state, which seems to be a failure of the semiempirical method. As in the other plots the minimum energy reaction path is observed starting in the lower right corner traveling horizontally to the left then upwards to the upper left corner.

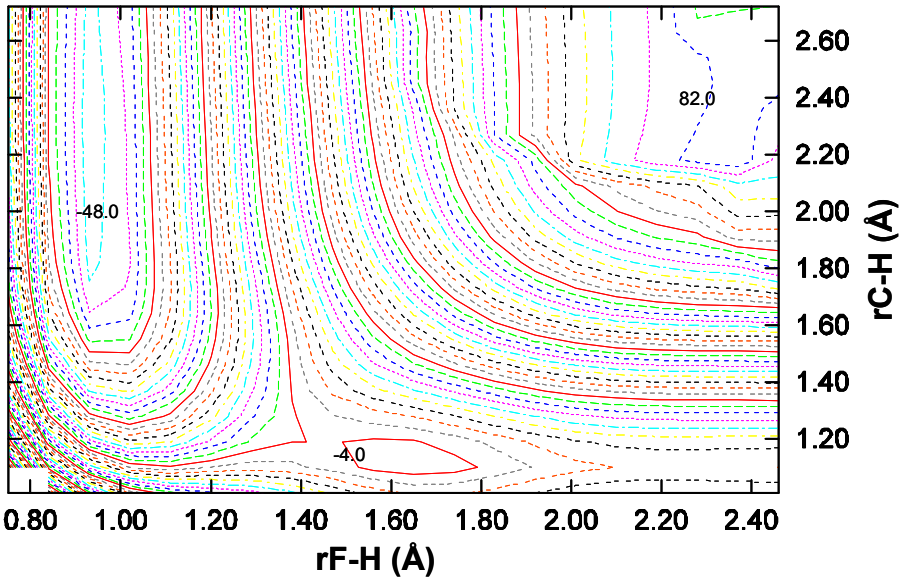

Figure 2.13. Potential energy surface scan for the reaction F + C_2H_6 → HF + C_2H_5 using PM3//MP2/aug-cc-pVDZ. Energy contours are plotted each 2 kcal/mol.

Chapter 3 Semiempirical Hamiltonian Parameter Fitting

The use of semiempirical theory in direct dynamics calculations diminishes the cost of using *ab initio* theory and negates the need for an analytical potential energy surface.[59] However, as seen in the previous section, semiempirical theory does not yield good agreement with experiments or high-level *ab initio* theory. This result is not very surprising, as the original parameters of the semiempirical Hamiltonians were not derived in order to describe F + alkane reactions. In this section, we describe how we have adjusted the parameters of the PM3 semiempirical Hamiltonian so that this method yields more accurate results for the reactions being studied.[59]

The parameters of PM3 Hamiltonian are optimized for F + alkanes using a nonlinear least-squares algorithm[60]. Only the parameters of H, C, and F are included in this optimization since they are the only relevant atoms to the reaction. Twenty-nine parameters in total are optimized. The parameters were adjusted to minimize the root mean squared deviation (RMSD) between the PM3 and a grid of *ab initio* energies covering different regions of the potential energy surfaces. The semiempirical energy is evaluated with a guess set of parameters. The initial guess set is the standard PM3 parameters. The differences between the *ab initio* energies and that set of energies are examined. First derivatives of the differences with respect to the parameters are taken numerically. A new set of parameters is obtained from the original set and the first derivatives of the differences between *ab initio* and semiempirical energies with respect to the parameters. The process was repeated until convergence.

The grid of *ab initio* points employed in the parameter optimization consists of 303 energies of the F + C_2H_6 → HF + C_2H_5 potential energy surface calculated at the CCSD(T)/aug-cc-pVDZ level. These points are from the IRC calculation, a scan of the C-H bond (1.1 Å - 2.8 Å, step size = 0.05Å) with the F-H-C angle held fixed at 180° and a scan of the F-H bond (0.95 Å - 2.2 Å, step size = 0.05Å) with the F-H-C bond held fixed at 180°, all optimized with MP2/aug-cc-pVDZ. There are 137 points from the reverse IRC, 101 points from the forward IRC, 35 points from the C-H scan and 26 points from the F-H scan.

Our first attempts provided sets of semiempirical parameters that produced trajectories with unphysical behavior. For instance, an F + C_2H_6 trajectory at 3.2 kcal/mol collision energy yielded FCH + CH_3 + H_2 as products, which is a reaction channel not open at such low energies. To further investigate this behavior, energies of snapshots of this nonphysical trajectory were calculated using MP2/aug-cc-pVDZ. As can be seen in Figure 3.1 there is good initial agreement between the MP2 and the preliminary SRP-PM3 energies. This region corresponds to the section of the trajectory in which reactants are approaching. However, the agreement between the preliminary SRP-PM3 and MP2 energies ceases in the region of strong interaction. The reason that this spurious behavior was seen in our initial Hamiltonian is the lack of points covering that region of the potential energy surface in the optimization procedure. To avoid this problem, we took the four points showing the greatest difference in MP2 and PM3 energy from this region of disparity, and included them in the fit.

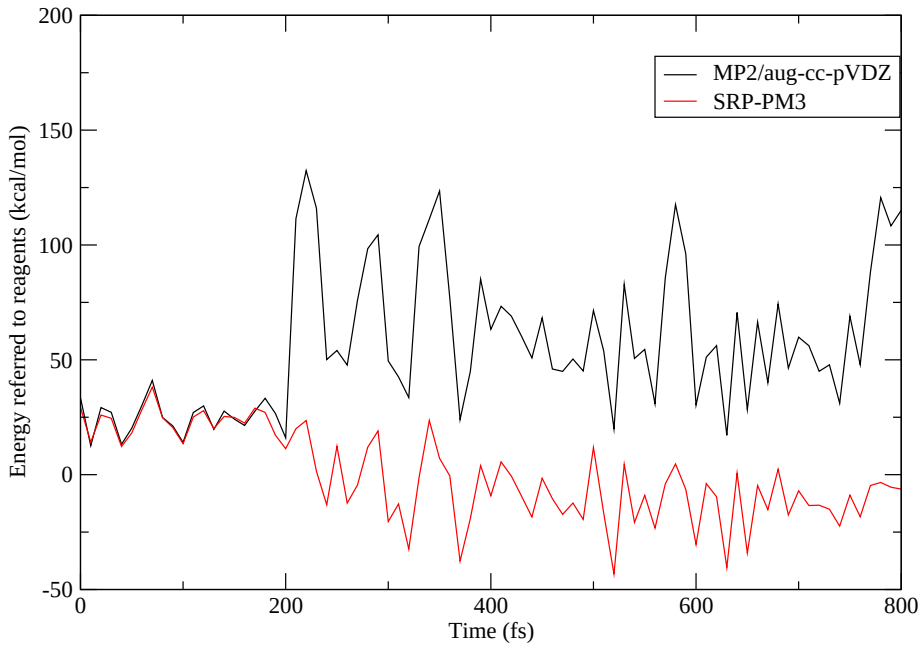

Figure 3.1. Comparison of the energies of a trajectory calculated with a preliminary SRP-PM3 and MP2/aug-cc-pVDZ.

The RMSD between the *ab initio* energies and the energies furnished by the PM3 Hamiltonian was 7.79 kcal/mol. After the fitting procedure was performed the new RMSD was 2.67 kcal/mol. As can be observed in Figure 3.2, there is a great improvement in the Hamiltonian's agreement with the *ab initio* energies. The $F + CH_4 \rightarrow HF + CH_3$ reaction energy for PM3-SRP is -28.39 kcal/mol. This energy is 16.15 kcal/mol higher than the initial PM3 energy of -44.54 kcal/mol. The new energy is about 3.7 kcal/mol above the experimental energy. The $F + C_2H_6 \rightarrow HF + C_2H_5$ reaction energy for PM3-SRP is -35.84 kcal/mol. This energy is 16.47 kcal/mol higher than the initial PM3 energy of -52.31 kcal/mol. The new reaction energy agrees with the experimental energies, with a difference of 0.1 – 0.5 kcal/mol.

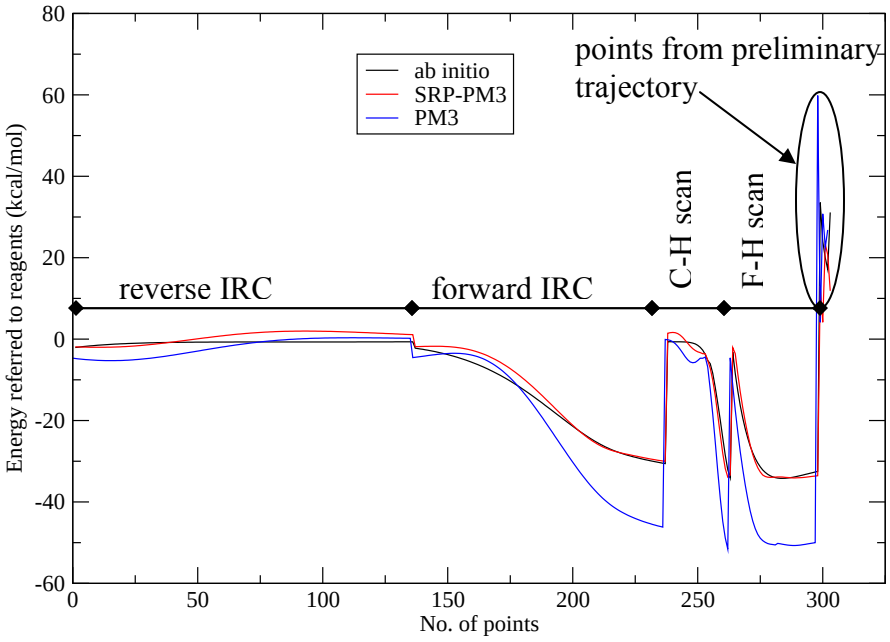

Figure 3.2. Comparison of the semiempirical and ab initio energies for the fit of PM3 parameters to CCSD(T)/aug-cc-pVDZ data.

A comparison of the parameters of the PM3 and SRP-PM3 semiempirical Hamiltonians are shown in Table 3.1. These parameters correspond to experimental values and approximate integrals used to represent electronic energy levels. It can be seen that not a large of amount of change is needed in the parameters to improve the

agreement with the *ab initio* data. The average change seen in the parameters is 4.7%. The most variance was seen in the β_s parameter of Hydrogen, a difference of 18.8%.

Figure 3.3 shows the IRC for $F + CH_4 \rightarrow HF + CH_3$ using MP2/aug-cc-pVDZ geometries. The IRC calculated with SRP-PM3 shows a decrease in the depth of the shallow well located between reagents and the transition state. The improvement in the reaction energy is also clearly evident. The SRP-PM3 IRC is in much better agreement with the CCSD(T) IRC than the original PM3. Figure 3.4 shows the IRC for $F + C_2H_6 \rightarrow HF + C_2H_5$ using MP2/aug-cc-pVDZ geometries. As with the previous reaction the depth of the PM3 well between reagents and transition state is decreased. And again the improvement in reaction energy is evident.

	PM3	SRP-PM3
Hydrogen		
U_{ss}	-13.0733210	-12.4488395
β_s	-5.6265120	-6.6837115
Z_s	0.9678070	1.0805484
α	3.3563860	3.0868163
G_{ss}	14.7942080	14.3606410
Carbon		
U_{ss}	-47.2703200	-49.1356733
U_{pp}	-36.2669180	-34.9167808
β_s	-11.9100150	-12.0800429
β_p	-9.8027550	-8.9305615
Z_s	1.5650850	1.7161182
Z_p	1.8423450	1.7638674
α	2.7078070	2.7081225
G_{ss}	11.2007080	10.4582627
G_{sp}	10.2650270	10.0018242
G_{pp}	10.7962920	10.6937958
G_{p2}	9.0425660	8.9341220
H_{sp}	2.2909800	2.1320118
Fluorine		
U_{ss}	-110.4353030	-109.1925741
U_{pp}	-105.6850470	-106.6935279
β_s	-48.4059390	-47.8963388
β_p	-27.7446600	-26.5166622
Z_s	4.7085550	5.0479742
Z_p	2.4911780	2.6907950
α	3.3589210	3.2150562
G_{ss}	10.4966670	11.1826051
G_{sp}	16.0736890	15.8832633
G_{pp}	14.8172560	14.1737776
G_{p2}	14.4183930	14.3310098
H_{sp}	0.7277630	0.7219357

Table 3.1. Comparison of PM3 and SRP-PM3 parameters

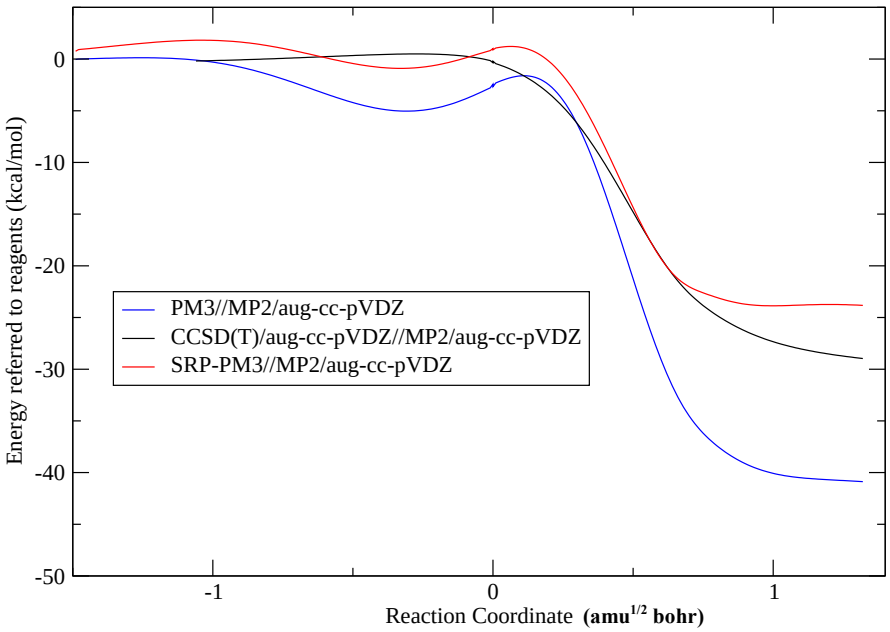

Figure 3.3. Intrinsic reaction coordinate for the F + CH_4 → HF + CH_3 reaction including SRP-PM3.

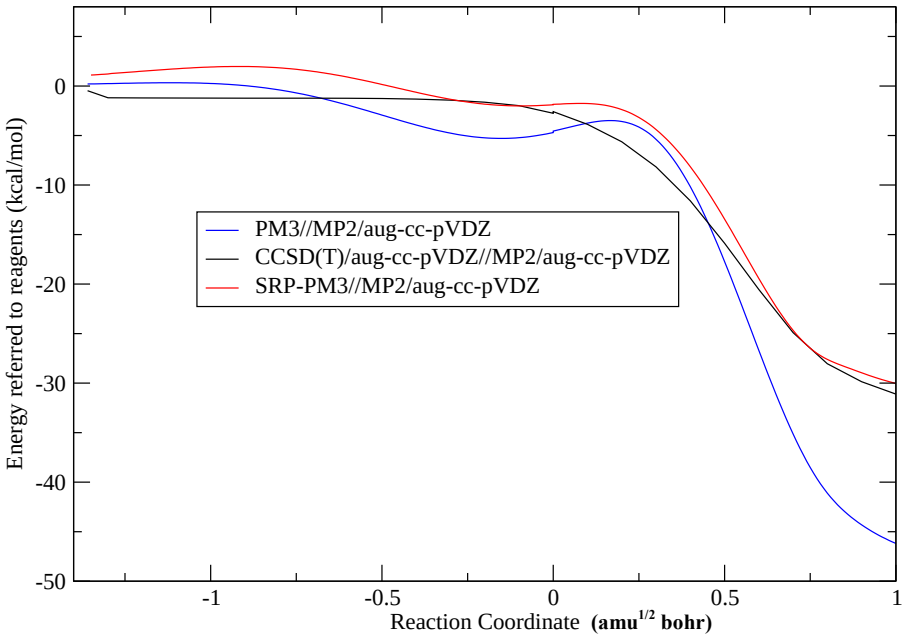

Figure 3.4. Intrinsic reaction coordinate for the F + C_2H_6 → HF + C_2H_5 reaction including SRP-PM3.

PES scans were performed with the new PM3 parameters. The energies are calculated for MP2/aug-cc-pVDZ geometries. The F + CH_4 → HF + CH_3 surface (Figure 3.5) shows a shallower well in the transition state region compared with the original PM3 surface. The F + C_2H_6 → HF + C_2H_5 surface (Figure 3.6) shows a barely visible transition state, and the spurious well in the transition state region is not present.

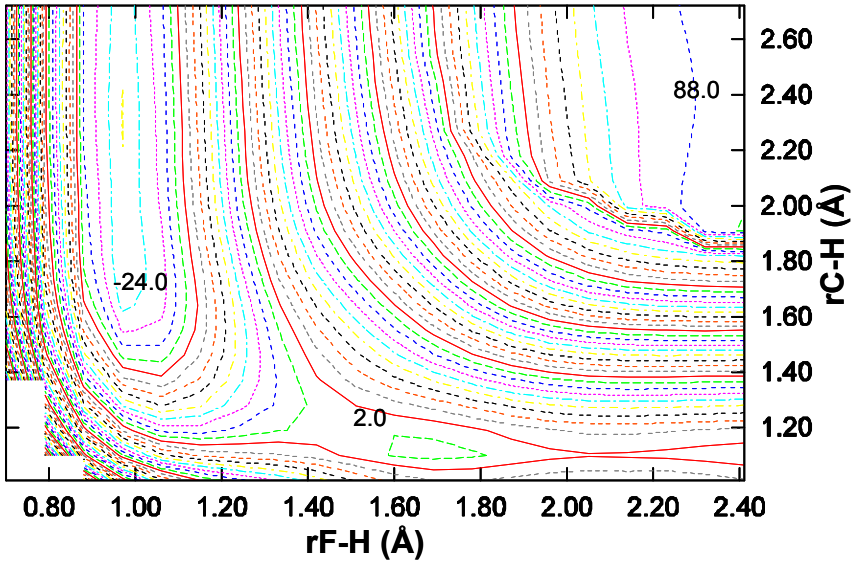

Figure 3.5. Potential energy surface scan for the reaction F + CH_4 → HF + CH_3 using SRP-PM3//MP2/aug-cc-pVDZ. Energy contours are plotted each 2 kcal/mol.

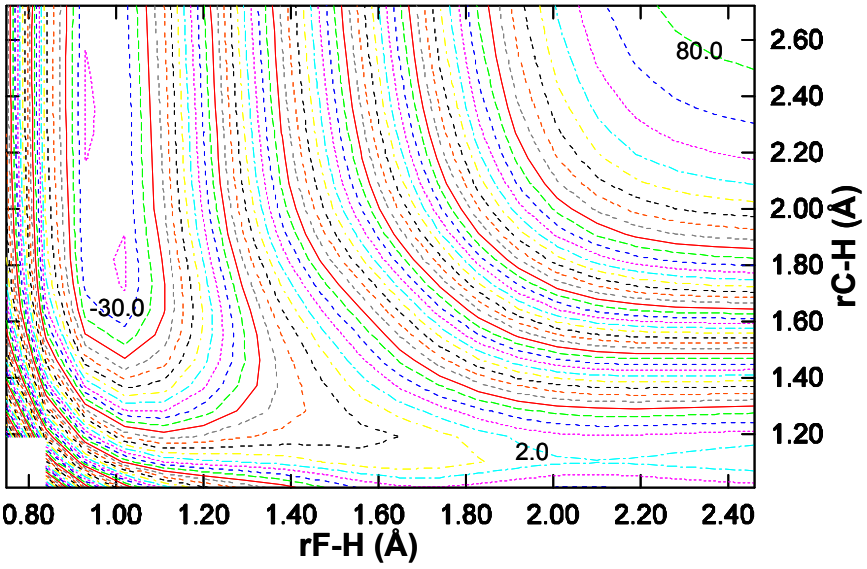

Figure 3.6. Potential energy surface scan for the reaction F + C_2H_6 → HF + C_2H_5 using SRP-PM3//MP2/aug-cc-pVDZ. Energy contours are plotted each 2 kcal/mol.

Chapter 4 Trajectory Calculations

To perform trajectory calculations initial conditions must first be generated. For the CH_4/C_2H_6 reactants, we do this by using the dynamical reaction coordinate (DRC)[61] function available in the GAMESS[62] package of programs. The DRC is a classical trajectory method based on quantum-mechanical potential energy surfaces. We use the VIBLVL option to give kinetic energy partitioned over the normal modes so that all of the normal modes receive energy corresponding to the zero-point at the beginning of the trajectory. The DRC code then provides initial coordinates and momenta corresponding to zero-point energy motion and a 'root' trajectory for only the molecule is propagated during 100000 steps of 0.1 fs. The instantaneous coordinates and momenta of various snapshots along that root trajectory are taken as initial coordinates for CH_4/C_2H_6. The coordinates and velocities of the F atom are then assigned taking into account the initial translational energy of the simulations, the maximum sampling impact parameter, and the initial distance between the F atom and the molecule. We have assigned an initial separation of F and CH_4/C_2H_6 of 10.0 bohrs. We have designated a maximum sampling impact of parameter of 6.5 bohrs and an initial translational energy of 0.07806 eV for the reaction $F + CH_4 \rightarrow HF + CH_3$. For $F + C_2H_6 \rightarrow HF + C_2H_5$ a maximum sampling impact parameter of 8.5 bohrs and an initial translational energy of 0.1388 eV have been used. These energies have been selected to allow for comparison with experiment[8, 37]. The maximum sampling impact parameters have been chosen to be large enough to capture all possible reactions taken place, but small enough that most trajectories do not result in inelastic or elastic scattering.

Once the initial conditions for the F radical and the molecules have been selected, each trajectory was then run with the DRC function of GAMESS. We note that we have modified GAMESS so that the semiempirical Hamiltonian described in Chapter 3 is used to compute the energy gradients required in the trajectory propagation. We calculated 4000 DRC points with a time step of 0.2 fs per trajectory. This is long enough that the system evolves from reactants to products, and trajectories are not stopped while the fragments are still interacting.

A Morse potential[63] was fit for the HF molecule using energies obtained with the SRP-PM3 Hamiltonian to allow for the study of vibrational and rotational distributions. These Morse potential parameters are used as described in Chapter 1 to calculate the vibrational and rotational quantum numbers for the HF molecule. The form of the Morse potential used is

$$E(r) = D_e(1 - \exp(-\beta(r - R_e)))^2 \tag{4.1}$$

where r is the internuclear distance, E is the energy at distance r, D_e is the depth of the potential minimum, R_e is the equilibrium internuclear distance, and β is defined by

$$\beta = \sqrt{\frac{k_e}{2D_e}} \tag{4.2}$$

where k_e is the bond force constant.

The HF internuclear distance was varied from 0.70Å to 5.00Å with a step size of 0.05Å except in the well region, where a step size of 0.01Å was used. The Morse potential was fit to the SRP-PM3 data using the nonlinear least squares fitting procedure described previously. The parameters were found to be: D_e = 0.167005 Hartree, β = 1.558716 bohr^{-1}, R_e = 1.73 bohr. The fitted Morse potential is shown in Figure 4.1. The fitted Morse potential can be used to calculate the constants shown in Table 4.1.

	ω_e	$\omega_e x_e$	B_e
SRP-PM3	4733.5	152.8	21.02
EXP[7]	4138.3	89.9	20.96

Table 4.1. Diatomic constants for the HF molecule.

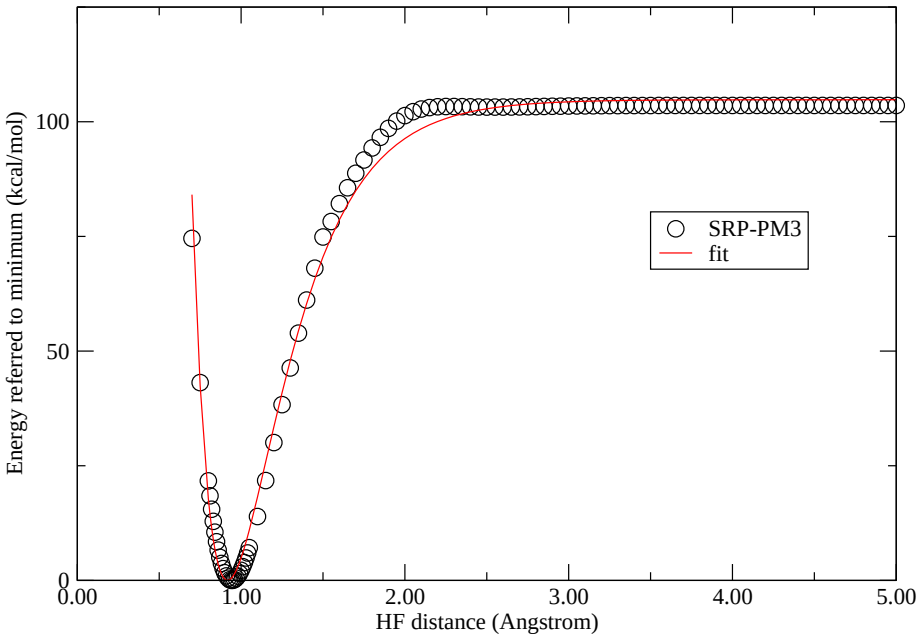

Figure 4.1. Plot of the Morse potential fitted to SRP-PM3 energies.

4.1 $F + CH_4 \rightarrow HF + CH_3$

Trajectory calculations were performed for the $F + CH_4 \rightarrow HF + CH_3$ reaction with a collision energy of 1.8 kcal/mol. The HF vibrational distributions obtained from our calculations are compared with experimental values shown in Figure 4.2. The figure also includes the results obtained with the original PM3 Hamiltonian and the analytical PES-NOSO surface available in the literature. The SRP-PM3 results are an improvement over the PM3 vibrational distribution. The PM3 distribution shows a peak at v=3 and a considerable population at v=0. SRP-PM3 shows a smaller v=0 population, similar to experiments. The HF distribution calculated with SRP-PM3 shows a peak at v=2 as seen in experiments. PES-NOSO shows a peak at v=1, in disagreement with experiment.

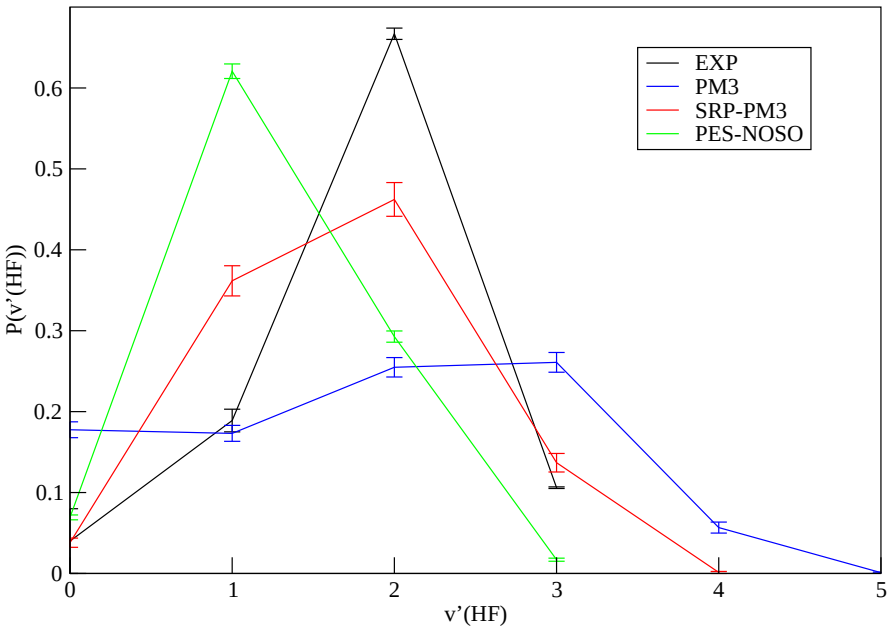

Figure 4.2. HF vibrational distributions for the F + CH_4 → HF + CH_3 reaction. Experimental data is from Nesbitt et al.[8]

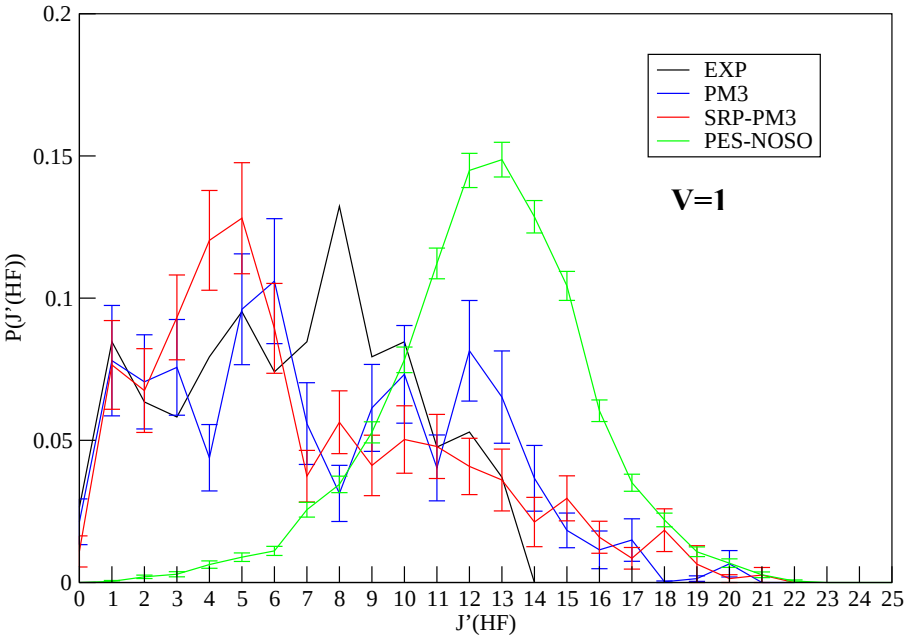

Figure 4.3. HF rotational distributions for the F + CH_4 → HF + CH_3 reaction at v=1. Experimental data is from Nesbitt et al.[8]

For the rotational distribution for HF (v=1) the PM3 and SRP-PM3 distributions are similar. Both are more excited than experiments. PES-NOSO is more rotationally excited than experiments or the other calculations with a peak around J=14. For HF (v=2), the experimental distribution shows a peak around J=2. PM3 and SRP-PM3 distributions are again similar. Both are slightly more rotationally excited than experiment but seem to show a peak around J=4. PES-NOSO is much more rotationally excited than experiment showing a peak around J=12, much higher than experiments. For HF (v=3) the experimental distribution shows a peak around J=1 and no population above J=7. As seen with v=1 and v=2 the PM3 and SRP-PM3 populations are similar, and are hotter than experiments. The PES-NOSO distribution is more excited than that of experiments PM3 and SRP-PM3.

For all of the HF rotational distributions PM3, SRP-PM3, and PES-NOSO distributions are more excited than experiments. PES-NOSO consistently shows a peak much higher than experiments. For all vibrational states the SRP-PM3 and PM3 rotational distributions are similar.

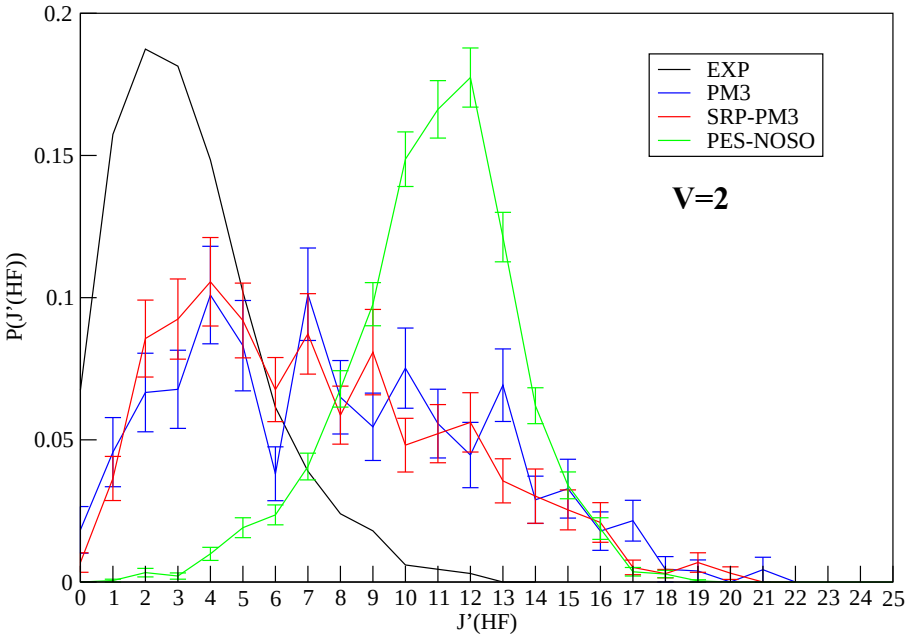

Figure 4.4. HF rotational distributions for the F + CH_4 → HF + CH_3 reaction at v=2. Experimental data is from Nesbitt et al.[8]

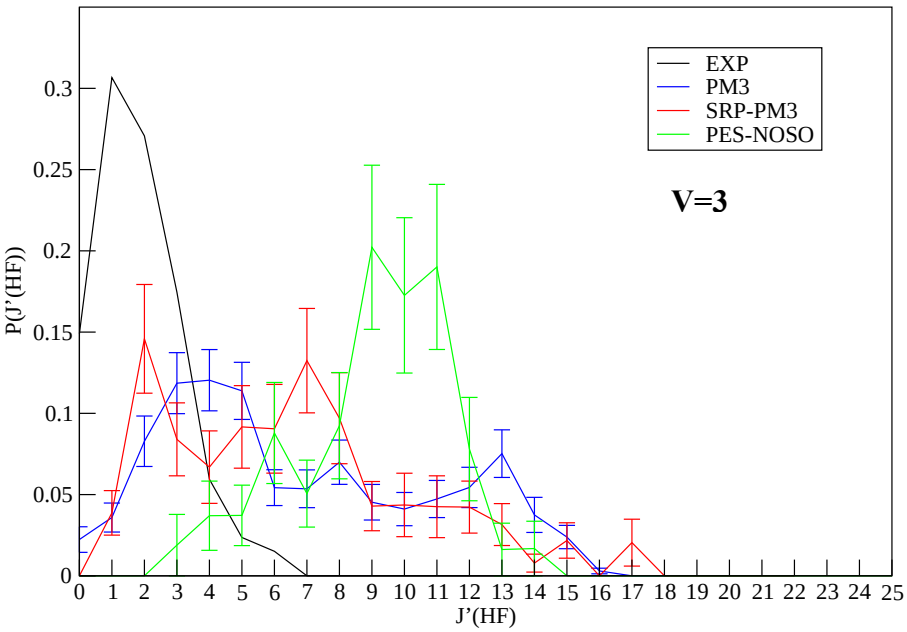

Figure 4.5. HF rotational distributions for the F + CH_4 → HF + CH_3 reaction at v=3. Experimental data is from Nesbitt et al.[8]

4.2 F + C_2H_6 → HF + C_2H_5

The calculated and experimental HF vibrational distributions are shown in Figure 4.6. As can be seen in the figure, all of the distributions peak at v=2. There are two main differences between PM3 and SRP-PM3 results. SRP-PM3 shows a population at v=2 that is much closer in agreement to experiments. Also SRP-PM3 shows a population in v=0 as does experiments while PM3 does not.

Let us turn our attention to the HF rotational distributions. For HF (v=1), the PM3 and SRP-PM3 distributions are quite similar, as seen with F + CH_4. These distributions also run much hotter than experiments with the highest populated state for experiments being J=13 and SRP-PM3 populating into J=29. For HF (v=2), a peak is seen in the experimental distribution at J=2. The calculated PM3 and SRP-PM3 distributions are similar, and notably more excited than experiment. For HF (v=3), the experiments only populate to J=10 with a peak at J=2. And again we see that PM3 and SRP-PM3 distributions are similar and much hotter than experiments.

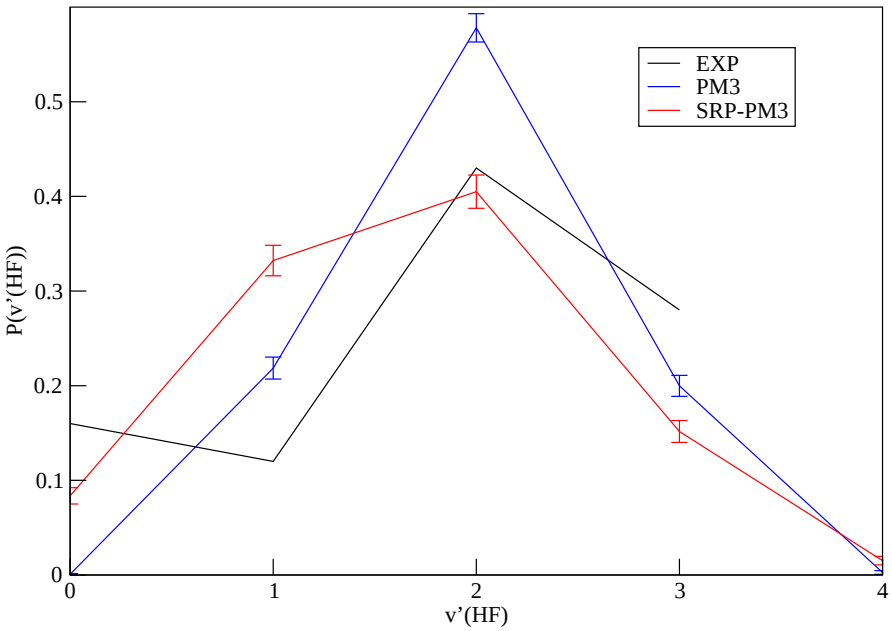

Figure 4.6. HF vibrational distributions for the F + C_2H_6 → HF + C_2H_5 reaction. Experimental data is from Nesbitt et al.[37]

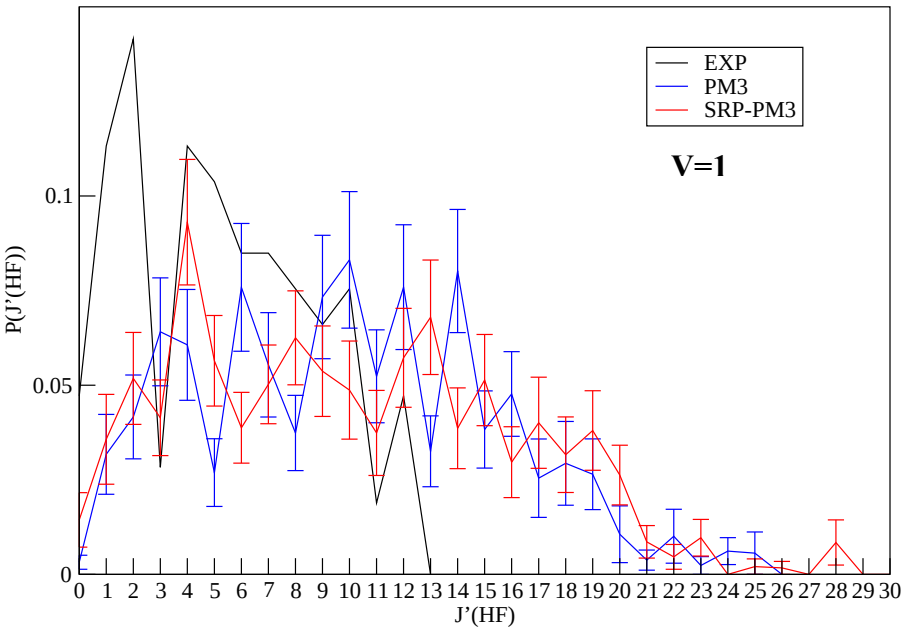

Figure 4.7. HF rotational distributions for the F + C_2H_6 → HF + C_2H_5 reaction at v=1. Experimental data is from Nesbitt et al.[37]

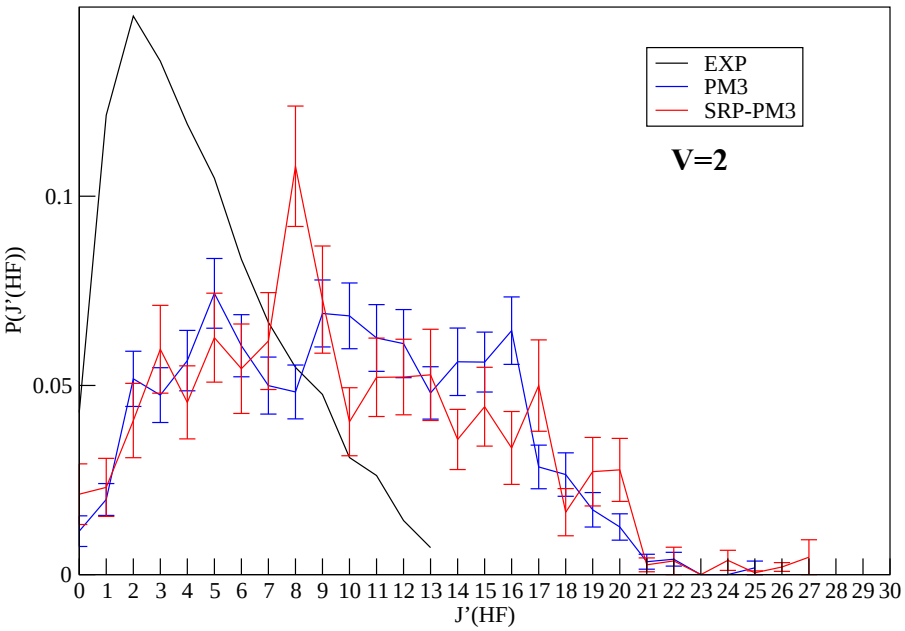

Figure 4.8. HF rotational distributions for the F + C_2H_6 → HF + C_2H_5 reaction at v=2. Experimental data is from Nesbitt et al.[37]

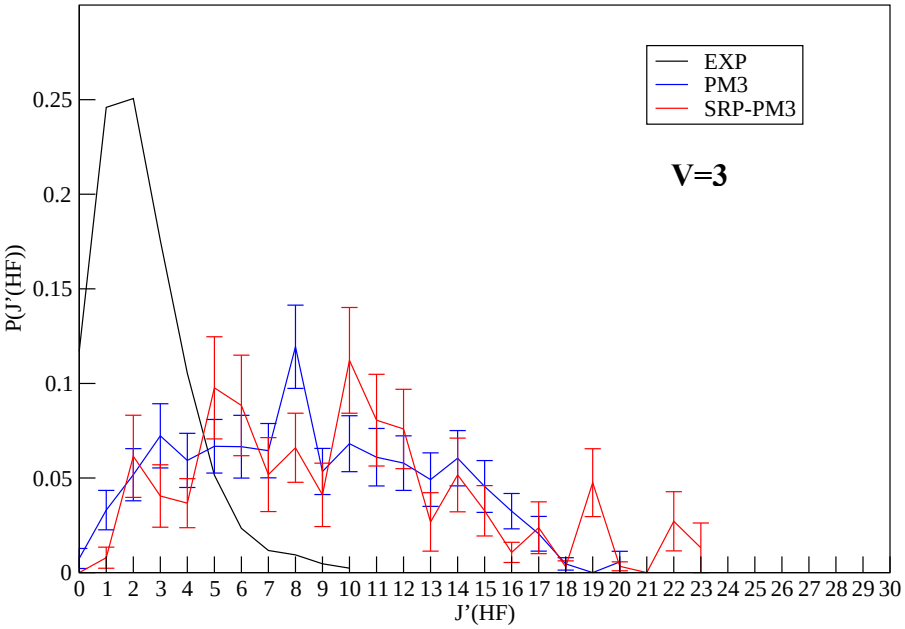

Figure 4.9. HF rotational distributions for the F + C_2H_6 → HF + C_2H_5 reaction at v=3. Experimental data is from Nesbitt et al.[37]

Overall, similar results are seen for all of the rotational distributions. PM3 and SRP-PM3 tend to show more rotational excitation than experiments. Also PM3 and SRP-PM3 show similar rotational distributions. These results indicate that although the semiempirical Hamiltonian that we have derived captures the broader aspects of the dynamics of the F + alkane reactions, it still is not able to provide predictive HF rotational distributions. It is likely that the difference between the calculated HF rotational distributions and experiment is not exclusively due to errors in the quality of the SRP Hamiltonian. In particular, it has been shown before that giving zero-point energy to the bending modes of alkane molecules in radical + alkane reactions leads to excessive product rotational distributions[64].

Chapter 5 Conclusions

5.1 Summary

The reactions between F radicals and the methane and ethane molecules have been studied at different levels of the chemical reaction theory. *Ab initio* calculations have been used to characterize the ground state potential energy surfaces. The *ab initio* information has then been used to reparametrize the PM3 Hamiltonian specifically for F+alkane reactions. Finally, quasiclassical trajectories have been carried out using the derived semiempirical Hamiltonian to learn about the dynamics of F + alkane reactions.

Through our *ab initio* study we have been able to see several things. The reaction energy can be accurately computed with dual-level CCSD(T) calculations, irrespective of the level at which geometries and harmonic frequencies are calculated. However, lower level geometries will probably not yield accurate results for the barrier when used in combination with CCSD(T) single-point calculations. This is true for both reactions. For the F + CH_4 reaction little to no barrier is observed with CCSD(T) theory. For the F + C_2H_6 reaction no barrier is observed. The reaction proceeds directly from products to reactants.

The fitting of the parameters of the PM3 Hamiltonian to *ab initio* data yielded improvement in the reaction energy. The improvement in the minimum reaction path and the potential energy surface scan showed that the new parameters have increased the agreement of PM3 with high level *ab initio* calculations. Our SRP-PM3 is able to improve the HF vibrational distributions for these reactions. However, the HF rotational distributions generated are virtually the same as those produced with PM3. Further adjustment of the PM3 parameters seems necessary to see improvement in the rotational distribution.

We conclude that the use of semiempirical Hamiltonians continues to be a viable way to perform trajectory calculations of large chemical reactions. The use of a single set of reaction parameters for multiple reactions seems also possible. With this option, the development of potential energy surfaces and trajectory studies can be streamlined. This is by no means a complete process but a start on an interesting technique.

5.2 Future Work

While this SRP-PM3 does improve the PM3 Hamiltonian, it is believed that better agreement with experiments can be achieved. The dynamics study can be expanded to include other properties and the deuterated analogue reactions. Further development could expand the reactions studied to include larger alkanes and self-assembled monolayers.

References

1. Espinosa-Garcia, J.; Bravo, J. L.; Rangel, C., New analytical potential energy surface for the F(P-2)+CH4 hydrogen abstraction reaction: Kinetics and dynamics. *Journal of Physical Chemistry A* **2007,** 111, (14), 2761-2771.

2. NIST Computational Comparison and Benchmark Database IVA Reaction Comparison Experimental Enthalpies at 0K. http://srdata.nist.gov/cccbdb

3. Nazar, M. A.; Polanyi, J. C., Energy-Distribution among Reaction-Products .14. F+Ch4, F+Ch3x (X=Cl,Br,I), F+Chncl4-N (N=1-3). *Chemical Physics* **1981,** 55, (3), 299-311.

4. Wickramaaratchi, M. A.; Setser, D. W.; Hildebrandt, H.; Korbitzer, B.; Heydtmann, H., Evaluation of HF product distributions deduced from infrared chemiluminiscence. II. F atom reactions. *Chemical Physics* **1985,** 94, (1-2), 109-129.

5. Sugawara, K. I.; Ito, F.; Nakanaga, T.; Takeo, H.; Matsumura, C., Vibrational and Rotational Energy-Distributions of CH3 and IF Formed in the Reactions of F-Atoms with CH4 and CH3I. *Journal of Chemical Physics* **1990,** 92, (9), 5328-5337.

6. Maneshkarimi, M.; Heydtmann, H., Infrared chemiluminescence in the systems F + CH4 and F + CH2F2. The effect of secondary reaction. *Chemical Physics Letters* **1995,** 234, (1-3), 182-186.

7. Harper, W. W.; Nizkorodov, S. A.; Nesbitt, D. J., Differential scattering dynamics of F+CH4 -> HF(v,J)+CH3 via high-resolution IR laser dopplerimetry. *Chemical Physics Letters* **2001,** 335, (5-6), 381-387.

8. Harper, W. W.; Nizkorodov, S. A.; Nesbitt, D. J., Quantum state-resolved reactive scattering of F+CH4 -> HF(v,J)+CH3: Nascent HF(v,J) product state distributions. *Journal of Chemical Physics* **2000,** 113, (9), 3670-3680.

9. Shiu, W.; Lin, J. J.; Liu, K. P.; Wu, M.; Parker, D. H., Imaging the pair-correlated excitation function: The F+CH4 -> HF(v ')+CH3 (v=0) reaction. *Journal of Chemical Physics* **2004,** 120, (1), 117-122.

10. Shiu, W.; Lin, J. J.; Liu, K. P., Reactive resonance in a polyatomic reaction. *Physical Review Letters* **2004,** 92, (10).

11. Merritt, J. M.; Rudic, S.; Miller, R. E., Infrared laser spectroscopy of CH3...HF in helium nanodroplets: The exit-channel complex of the F+CH4 reaction. *Journal of Chemical Physics* **2006,** 124, (8).

12. Fettis, G. C.; Knox, J. H.; Trotman-Dickenson, A. F., The Reactions of Fluorine Atoms with Alkanes. *Journal of the Chemical Society* **1960**, 1064-1071.

13. Foon, R.; Reid, G. P., Kinetics of the gas phase fluorination of hydrogen and alkanes. *Trans. Faraday Soc.* **1971,** 67, 3513 - 3520.

14. Williams, R. L.; Rowland, F. S., Hydrogen atom abstraction by fluorine atoms. *Journal of Physical Chemistry* **1973,** 77, (3), 301-307.

15. Chang, H. W.; Setser, D. W., Infrared chemiluminescence and energy partitioning from the reactions of fluorine atoms with the primary carbon-hydrogen bonds of alkanes, halogenated methanes, and tetramethyl silane. *Journal of Chemical Physics* **1973,** 58, (6), 2298-2309.

16. Bogan, D. J.; Setser, D. W., HF infrared chemiluminescence: Energy disposal and the role of the radical fragment in the abstraction of hydrogen from polyatomic molecules by F atoms. *Journal of Chemical Physics* **1976,** 64, (2), 586-602.

17. Smith, D. J.; Setser, D. W.; Kim, K. C.; Bogan, D. J., HF infrared chemiluminescence. Relative rate constants for hydrogen abstraction from hydrocarbons, substituted methanes, and inorganic hydrides. *Journal of Physical Chemistry* **1977,** 81, (9), 898-905.

18. Moore, C.; Smith, I. W. M., Rate Constants for the Reactions of Fluorine-Atoms with Alkanes and Hydrofluorocarbons at Room-Temperature. *Journal of the Chemical Society-Faraday Transactions* **1995,** 91, (18), 3041-3044.

19. Persky, A., Kinetics of the F+CH4 reaction in the temperature range 184-406 K. *Journal of Physical Chemistry* **1996,** 100, (2), 689-693.

20. Persky, A., The temperature dependence of the kinetic isotope effect in the reaction of F atoms with CH4 and CD4. *Chemical Physics Letters* **2006,** 430, (4-6), 251-254.

21. Gauss, A., Trajectory calculations on the fluorine methane chemical laser reaction. *Journal of Chemical Physics* **1976,** 65, (11), 4365-4369.

22. Davis, L. P.; Burggraf, L. W.; Gordon, M. S.; Baldridge, K. K., A theoretical study of fluorine atom and fluoride ion attack on methane and silane. *Journal of the American Chemical Society* **1985,** 107, (15), 4415-4419.

23. Kornweitz, H.; Persky, A.; Levine, R. D., The exoergic F+CH4 reaction as an example of peripheral dynamics. *Chemical Physics Letters* **1998,** 289, (1-2), 125-131.

24. Corchado, J. C.; Espinosa-Garcia, J., Theoretical study of the CH_4+F --> CH_3+FH reaction. I. Ab initio reaction path. *Journal of Chemical Physics* **1996,** 105, (8), 3152-3159.

25. Corchado, J. C.; Espinosa-Garcia, J., Theoretical study of the CH_4+F --> CH_3+FH reaction. II. Semiempirical surfaces. *Journal of Chemical Physics* **1996,** 105, (8), 3160-3167.

26. Joseph, T.; Steckler, R.; Truhlar, D. G., A new potential energy surface for the CH_3+H_2 <--> CH_4+H reaction: Calibration and calculations of rate constants and kinetic isotope effects by variational transition state theory and semiclassical tunneling calculations. *Journal of Chemical Physics* **1987,** 87, (12), 7036-7049.

27. Troya, D.; Millan, J.; Banos, I.; Gonzalez, M., Ab initio potential energy surface, variational transition state theory, and quasiclassical trajectory studies of the F+CH4 -> HF+CH3 reaction. *Journal of Chemical Physics* **2004,** 120, (11), 5181-5191.

28. Roberto-Neto, O.; Machado, F. B. C.; Ornellas, F. R., Transition state structure, energetics, and rate constants for the CH4+F(P-2)-> CH3+HF reaction. *Chemical Physics* **2005,** 315, (1-2), 27-34.

29. Rangel, C.; Navarrete, M.; Espinosa-Garcia, J., Potential energy surface for the F(P-2(3/2),P-2(1/2))+CH4 hydrogen abstraction reaction. Kinetics and dynamics study. *Journal of Physical Chemistry A* **2005,** 109, (7), 1441-1448.

30. Espinosa-Garcia, J., New analytical potential energy surface for the CH_4 + H hydrogen abstraction reaction: Thermal rate constants and kinetic isotope effects. *Journal of Chemical Physics* **2002,** 116, (24), 10664-10673.

31. Troya, D., Ab initio and direct quasiclassical-trajectory study of the F+CH4 -> HF+CH3 reaction. *Journal of Chemical Physics* **2005,** 123, (21).

32. Castillo, J. F.; Aoiz, F. J.; Banares, L.; Martinez-Nunez, E.; Fernandez-Ramos, A.; Vazquez, S., Quasiclassical trajectory study of the F+CH4 reaction dynamics on a

dual-level interpolated potential energy surface. *Journal of Physical Chemistry A* **2005,** 109, (38), 8459-8470.

33. Chu, T. S.; Zhang, X.; Ju, L. P.; Yao, L.; Han, K. L.; Wang, M. L.; Zhang, J. Z. H., First principles quantum dynamics study reveals subtle resonance in polyatomic reaction: The case of F+CH4 -> HF+CH3. *Chemical Physics Letters* **2006,** 424, (4-6), 243-246.

34. Wang, Q.; Cai, Z. T.; Feng, D. C., Reactive resonance and formation mechanism of the F+CH4 -> HF+CH3 reaction. *Journal of Molecular Structure-Theochem* **2006,** 759, (1-3), 31-34.

35. Maricq, M. M.; Szente, J. J., A Kinetic Study of the Reaction between Ethylperoxy Radicals and HO2. *Journal of Physical Chemistry* **1994,** 98, (8), 2078-2082.

36. Persky, A., The temperature dependence of the rate constant for the reaction F+C2H6. *Chemical Physics Letters* **2003,** 380, (3-4), 286-291.

37. Whitney, E. S.; Zolot, A. M.; McCoy, A. B.; Francisco, J. S.; Nesbitt, D. J., Reactive scattering dynamics in atom plus polyatomic systems: F+C2H6 -> HF(v,J)+C2H5. *Journal of Chemical Physics* **2005,** 122, (12).

38. Bottoni, A.; Poggi, G., An Ab-Initio Study of Hydrogen Abstraction by Fluorine, Chlorine and Bromine Atoms from Ethane and Propane. *Theochem-Journal of Molecular Structure* **1995,** 337, (2), 161-172.

39. Hirst, D. M., *Potential Energy Surfaces: Molecular Structure & Reaction Dynamics*. Taylor & Francis: London, 1985.

40. Bolton, K.; Hase, W. L.; Peslherbe, G. H., Direct Dynamics Simulations of Reactive Systems. In *Modern Methods for Multidimensional Dynamics Computations in Chemistry*, Thompson, D. L., Ed. World Scientific: Singapore, 1998; pp 143-189.

41. Brouard, M., *Reaction Dynamics*. Oxford University Press: Oxford, 1998.

42. Levine, R. D., *Molecular Reaction Dynamics*. Cambridge University Press: 2005.

43. Porter, R. N.; Raff, L. M., Classical Trajectory Methods in Molecular Collisons. In *Dynamics of Molecular Collisons Part B*, Miller, W. H., Ed. Plenum Press: New York, 1976; pp 1-52.

44. Hollas, J. M., *Modern Spectroscopy*. John Wiley & Sons, Ltd: 2004.

45. Møller, C.; Plesset, M. S., Note on an Approximation Treatment for Many-Electron Systems. *Physical Review* **1934,** 46, (7), 618.

46. Becke, A. D., Density-Functional Thermochemistry .3. the Role of Exact Exchange. *Journal of Chemical Physics* **1993,** 98, (7), 5648-5652.

47. Lee, C. T.; Yang, W. T.; Parr, R. G., Development of the Colle-Salvetti Correlation-Energy Formula into a Functional of the Electron-Density. *Physical Review B* **1988,** 37, (2), 785-789.

48. Crawford, T. D.; Schaefer, H. F., An Introduction to Coupled Cluster Theory for Computational Chemists. In *Reviews in Computational Chemistry*, Kenny B. Lipkowitz, D. B. B., Ed. 2007; pp 33-136.

49. Stewart, J. J. P., Optimization of parameters for semiempirical methods I. Method. *Journal of Computational Chemistry* **1989,** 10, (2), 209-220.

50. Dewar, M. J. S.; Zoebisch, E. G.; Healy, E. F.; Stewart, J. J. P., Development and use of quantum mechanical molecular models. 76. AM1: a new general purpose quantum mechanical molecular model. *Journal of the American Chemical Society* **1985,** 107, (13), 3902-3909.

51. Ahlswede, B.; Jug, K., Consistent modifications of SINDO1: I. Approximations and parameters. *Journal of Computational Chemistry* **1999,** 20, (6), 563-571.

52. Dunning, T. H., Gaussian basis sets for use in correlated molecular calculations. I. The atoms boron through neon and hydrogen. *Journal of Chemical Physics* **1989,** 90, (2), 1007-1023.

53. Halkier, A.; Helgaker, T.; Jorgensen, P.; Klopper, W.; Koch, H.; Olsen, J.; Wilson, A. K., Basis-set convergence in correlated calculations on Ne, N2, and H2O. *Chemical Physics Letters* **1998,** 286, (3-4), 243-252.

54. NIST Chemistry WebBook. http://webbook.nist.gov/chemistry/

55. Thermodynamic Data. http://www.iupac-kinetic.ch.cam.ac.uk/Thermo2003.pdf

56. Sander, S. P., B. J. Finlayson-Pitts, R. R. Friedl, D. M. Golden, R. E. Huie, H. Keller-Rudek, C. E. Kolb, M. J.; Kurylo, M. J. M., G. K. Moortgat, V. L. Orkin, A. R. Ravishankara and P. H. Wine *Chemical Kinetics and Photochemical Data for Use in Atmospheric Studies, Evaluation Number 15*; Jet Propulsion Laboratory: Pasadena, 2006.

57. Frisch, M. J.; Trucks, G. W.; Schlegel, H. B.; Scuseria, G. E.; Robb, M. A.; Cheeseman, J. R.; Montgomery, J. A.; Vreven, T.; Kudin, K. N.; Burant, J. C.; Millam, J. M.; Iyengar, S. S.; Tomasi, J.; Barone, V.; Mennucci, B.; Cossi, M.; Scalmani, G.; Rega, N.; Petersson, G. A.; Nakatsuji, H.; Hada, M.; Ehara, M.; Toyota, K.; Fukuda, R.; Hasegawa, J.; Ishida, M.; Nakajima, T.; Honda, Y.; Kitao, O.; Nakai, H.; Klene, M.; Li, X.; Knox, J. E.; Hratchian, H. P.; Cross, J. B.; Bakken, V.; Adamo, C.; Jaramillo, J.; Gomperts, R.; Stratmann, R. E.; Yazyev, O.; Austin, A. J.; Cammi, R.; Pomelli, C.; Ochterski, J. W.; Ayala, P. Y.; Morokuma, K.; Voth, G. A.; Salvador, P.; Dannenberg, J. J.; Zakrzewski, V. G.; Dapprich, S.; Daniels, A. D.; Strain, M. C.; Farkas, O.; Malick, D. K.; Rabuck, A. D.; Raghavachari, K.; Foresman, J. B.; Ortiz, J. V.; Cui, Q.; Baboul, A. G.; Clifford, S.; Cioslowski, J.; Stefanov, B. B.; Liu, G.; Liashenko, A.; Piskorz, P.; Komaromi, I.; Martin, R. L.; Fox, D. J.; T. Keith; Al-Laham, M. A.; Peng, C. Y.; Nanayakkara, A.; Challacombe, M.; Gill, P. M. W.; Johnson, B.; Chen, W.; Wong, M. W.; Gonzalez, C.; Pople, J. A. *Gaussian 03*, Gaussian, Inc.: Wallingford CT, 2004.

58. Gonzalez, C.; Schlegel, H. B., An improved algorithm for reaction path following. *The Journal of Chemical Physics* **1989,** 90, (4), 2154-2161.

59. Gonzalez-Lafont, A.; Truong, T. N.; Truhlar, D. G., Direct dynamics calculations with NDDO (neglect of diatomic differential overlap) molecular orbital theory with specific reaction parameters. *Journal of Physical Chemistry* **1991,** 95, (12), 4618-4627.

60. http://netlib.org/

61. Taketsugu, T.; Gordon, M. S., Dynamic Reaction Coordinate Analysis: An Application to SiH4 + H- →. SiH5. *Journal of Physical Chemistry* **1995,** 99, (21), 8462-8471.

62. Schmidt, M. W.; Baldridge, K. K.; Boatz, J. A.; Elbert, S. T.; Gordon, M. S.; Jensen, J. H.; Koseki, S.; Matsunaga, N.; Nguyen, K. A.; Su, S.; Windus, T. L.; Dupuis, M.; John A. Montgomery, J., General atomic and molecular electronic structure system. *Journal of Computational Chemistry* **1993,** 14, (11), 1347-1363.

63. Morse, P. M., Diatomic Molecules According to the Wave Mechanics. II. Vibrational Levels. *Physical Review* **1929,** 34, (1), 57.

64. Troya, D.; Weiss, P. J. E., Ab initio and direct quasiclassical-trajectory study of the Cl+CH4 -> HCl+CH3 reaction. *Journal of Chemical Physics* **2006,** 124, (7).